AD-A083 390 NAVAL RESEARCH LAB WASHINGTON DC F/G 20/9
THE 24 INCH CUSP EXPERIMENT.(U)
FEB 80 R E PECHACEK, J R GREIG, M RALEIGH
UNCLASSIFIED NRL-MR-4162 SBIE-AD-E000 389 NL

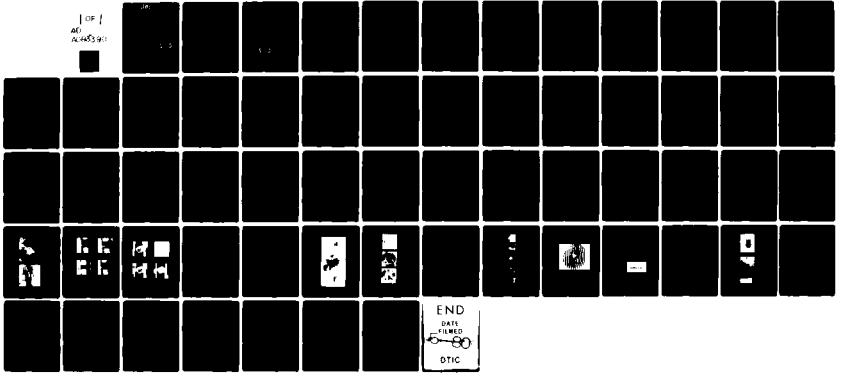

END
DATE FILMED
DTIC

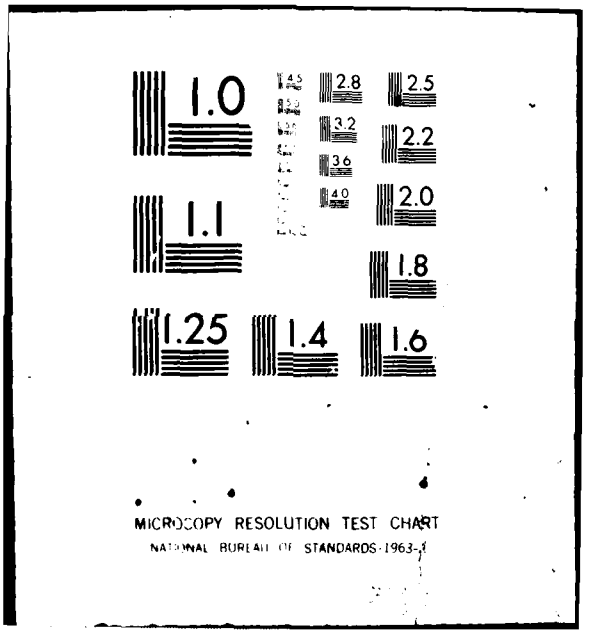
1.0
2.8
2.5
3.2
2.2
3.6
4.0
2.0
1.1
1.8
1.25
1.4
1.6
MICROCOPY RESOLUTION TEST CHART
NATIONAL BUREAU OF STANDARDS-1963-A

(12) LEVEL III

ade 000 389

NW

NRL Memorandum Report 4162

The 24" CUSP Experiment

R. E. PECHACEK, J. R. GREIG AND M. RALEIGH

Experimental Plasma Physics Branch

AND

D. W. KOOPMAN AND A. W. DESILVA

University of Maryland
College Park, Maryland 20742

February 15, 1980

NAVAL RESEARCH LABORATORY
Washington, D.C.

SECURITY CLASSIFICATION OF THIS PAGE (When Data Entered)

REPORT DOCUMENTATION PAGE		READ INSTRUCTIONS BEFORE COMPLETING FORM
1. REPORT NUMBER NRL Memorandum Report 4162	2. GOVT ACCESSION NO. AD-A083 390	3. RECIPIENT'S CATALOG NUMBER
4. TITLE (and Subtitle) THE 24" CUSP EXPERIMENT		5. TYPE OF REPORT & PERIOD COVERED Final report on an NRL problem. 6. PERFORMING ORG. REPORT NUMBER
7. AUTHOR(s) R. E. Pechacek, J. R. Greig, M. Raleigh, D. W. Koopman*, and A. W. DeSilva*		8. CONTRACT OR GRANT NUMBER(s)
9. PERFORMING ORGANIZATION NAME AND ADDRESS Naval Research Laboratory Washington, DC 20375		10. PROGRAM ELEMENT, PROJECT, TASK AREA & WORK UNIT NUMBERS NRL Problem 67-0871-0-0 Project RR 011-09-41
11. CONTROLLING OFFICE NAME AND ADDRESS Office of Naval Research Arlington, VA 22217		12. REPORT DATE February 15, 1980 13. NUMBER OF PAGES 60
14. MONITORING AGENCY NAME & ADDRESS(if different from Controlling Office)		15. SECURITY CLASS. (of this report) UNCLASSIFIED 15a. DECLASSIFICATION/DOWNGRADING SCHEDULE

16. DISTRIBUTION STATEMENT (of this Report)

Approved for public release; distribution unlimited.

17. DISTRIBUTION STATEMENT (of the abstract entered in Block 20, if different from Report)

18. SUPPLEMENTARY NOTES

*University of Maryland, College Park, Maryland 20742

19. KEY WORDS (Continue on reverse side if necessary and identify by block number)

CUSP

20. ABSTRACT (Continue on reverse side if necessary and identify by block number)

A spectroscopically pure, fully ionized D_2 plasma containing 2×10^{19} ions is generated from solid D_2 pellets using a sequence of a 100 J Nd-Glass laser pulse and a 1000 J CO_2 laser pulse. The plasma is used to fill a cusp configured magnetic field with a $\beta = 1$ plasma. The width of the ring cusp is determined using laser scattering techniques. The laser scattering result, which agrees with chamber wall light emission and chemical deposits, is that the ring cusp is an ion Larmor radius wide, in contrast to recent experiments that have indicated that the cusp width is considerably narrower.

DD FORM 1 JAN 73 1473 EDITION OF 1 NOV 65 IS OBSOLETE
S/N 0102-014-6601

SECURITY CLASSIFICATION OF THIS PAGE (When Data Entered)

Contents

I. INTRODUCTION

The 24" CUSP experiment was originally undertaken for two purposes: The first was to develop a technique for making a large volume of warm plasma, which might be used as the initial plasma for an imploding liner experiment. The second purpose was to study the confinement of this plasma in a cusp configured magnetic bottle in an attempt to relieve the controversy over the width of the cusp through which plasma escapes. The plasma production method was ideal for this task since it produced a single species $\beta = 1$ plasma; the width of the cusp was measured by means of scattering diagnostic techniques.

The surface of a plasma contained in a cusp-configured magnetic bottle is everywhere concave toward the magnetic field. See Fig.1. Like any closed surface that is everywhere concave outward, the plasma surface must have some points or edges. The concave outward plasma surface is magnetohydrodynamically (MHD) stable, and for this reason the magnetic cusp was one of the first configurations considered for a fusion reactor. The principal disadvantage is that the points or edges, which are called "cusps", are like holes in the magnetic field from which plasma is able to escape. These holes severely limit the usefulness of the magnetic cusp configuration and it is the size of these holes that is the object of the present study.

Note: Manuscript submitted November 7, 1979.

The cusp magnetic field was first considered in the 1950's before fusion research was declassified by the U.S. and the U.S.S.R. Cusp containment research from this beginning up to 1971 was reviewed in 1971 by Spalding.[1] In 1977 Haines[2] reviewed the research from 1971 to that year. The gist of the research up to and including 1971 can be summarized as follows: Theoretically, the cusp hole size is computed to be of the order of an electron gyroradius if electric fields are allowed to exist in the plasma-magnetic field interface. If electric fields are not allowed, the hole size is of the order of an ion gyroradius, a factor of 60 larger than the $E \neq 0$ case. In early experiments[3] the hole size was estimated to be of the order of an ion gyroradius. The ion gyroradius cusp width remained unchallenged, experimentally, until 1974, when Kitsunezaki,[4] et al., using a laser produced D_2 plasma, claimed the cusp width to be of the order of a hybrid gyroradius for a $\beta = 1$ plasma. A year later, Hershkowitz,[5] et al., using an array of line cusps and a very low β plasma also measured the cusp width to be a hybrid gyroradius. Most recently, 1978, the same research group that was cited in Ref. 4 repeated the cusp containment experiment with a laser produced plasma, this time using polyethylene and aluminum targets.[6] The principal result of this experiment was that for $0.2 \leq \beta \leq 0.6$, the cusp half-width was from .6 to 2.9 times the ion Larmor radius. The cusp width measurement for a $\beta = 1$ plasma was not repeated for these plasmas.

Only two of the above mentioned experiments[3,4] involved measurements with $\beta = 1$ plasmas. In the case of the earlier experiment, the plasma was generated by plasma guns and the possibility existed that currents from the guns passed through the plasma, thereby reducing the plasma β and enhancing the plasma loss rate. In the case of the second experiment, the apparatus was very small and spatial resolution difficult. Also both of the above experiments measured the cusp width with probes, which may interfere with the plasma. The present experiment removes these sources of doubt by using a laser-produced plasma that can have no wall-connected currents, by using a large plasma in which the ion gyroradius was $\sim$ 1. cm, and by measuring the cusp width directly by laser scattering. A diamagnetic loop monitors the position of the plasma-magnetic field interface as a function of time and affirms that the magnetic field is completely excluded from the plasma, i.e. $\beta = 1$.

The remainder of this report is organized as follows: In the next section, the method of making and dropping the deuterium pellets is described. Then the optical alignment system and procedure for dropping the pellets into the focus of a laser beam is discussed. In the fourth section, the two-laser plasma generation system and the properties of the resulting plasma are described. In the fifth section the results of the cusp experiment are presented and in the sixth section those results are compared with those of other researchers and conclusions drawn.

II. DEUTERIUM PELLET MAKING AND DROPPING SYSTEM

An unambiguous measurement of the cusp width for a $\beta = 1$ plasma, in terms of the plasma gyroradii, puts two restrictions on the properties of that plasma. First, the plasma must contain only a single ion species, so that there is only one ion gyroradius to contend with. This limits the choice of plasmas to a clean hydrogen plasma. Second the plasma must not contain any imbedded magnetic fields of the kind that may be generated in electrical discharge created plasmas. In particular, there must not be any magnetic field lines in the plasma that connect to the vacuum chamber wall, as these lines would be a possible escape route for the plasma. Both of these restrictions are met by a plasma produced from a hydrogen (or deuterium) pellet by laser irradiation. Since such a plasma starts from a very small volume it can be created at the null at the center of the already established cusp field without enclosing a significant amount of the field. Also, it does not contain any of the impurities associated with electrodes or with discharges that originate on chamber walls.

The method used to produce the deuterium pellets was first developed in Garching by a group under Salvat.[7] A filament of solid deuterium is extruded and then cut to pellet length by a pair of resistively heated wires. The extrusion of solid D_2 filaments for laser plasma experiments was first accomplished by Friedman,[8] and it is his extruder that was used in this

experiment. Figure 2 is a mechanical drawing of Friedman's deuterium extruder. The extruder was modified for the present experiment by soldering a coil of copper tubing into the liquid helium reservoir. In order to achieve accurate pellet dropping, the D_2 filament must be considerably warmer than the $4.2^{o}K$ of liquid helium. Instead of using liquid helium, the extruder is chilled with cold helium gas flowing through the copper coil. The extruder temperature can be coarsely controlled by regulating the flow of cold helium gas.

A schematic diagram of the extruder chilling system is shown in Fig. 3. Helium gas flows directly from a 50 liter storage dewar, through a transfer tube, to the coil of copper tubing in the extruder reservoir. The rate of helium flow is controlled by the power applied to a resistive heater in the liquid helium. The rate of helium evaporation is 1.4 liters/hour/watt. The end of the transfer tube in the storage dewar is made of copper and maintained at liquid helium temperature by contact with the liquid. This contact insures that the temperature of the gas that enters the transfer tube will be very near $4.2^{o}K$.

The extruder cooling procedure is as follows: The liquid nitrogen reservoir and the inner reservoir, which now contains a coil of copper tubing, are filled with liquid nitrogen. When the temperature of the extruder has stabilized at $77^{o}K$, the LN_2 is blown out of the inner reservoir, and that reservoir is evacuated

by a mechanical pump to a pressure of about .05 torr. It is important that nearly all of the LN_2 be blown out of the reser voir before pumping. Pumping will cause the LN_2 to freeze and solid nitrogen has a very low vapor pressure. Freezing can be avoided by monitoring the extruder temperature during the pumping. If the temperature drops significantly, the pumping can be stopped and the remaining LN_2 blown out of the reservoir. After the LN_2 has been removed from the reservoir, it is filled with room temperature helium and the transfer tube to the storage dewar is connected. About 30 watts of 60 cycle power is then applied to the storage dewar heating element (a coil of 150μ diameter manganin wire wound on a nylon spool). The resulting rapid flow of cold helium into and through the extruder assembly, brings its temperature to 5 - 7^{o}K *in about* ten minutes. As the temperature nears 7^{o}K, the gas flow is manually reduced to reach a steady state with a small flow.rate. (A 50 liter dewar lasts about 3 hours.) At this point, the extruder is ready to be filled with D_2.

With the ram raised (See Figure 2), D_2 is bled into the extruder block through a needle valve, from a 500 cm^3 reservoir filled to a pressure of 40 psi. The room temperature D_2 is a large heat load on the extruder and the cold helium gas flow must be increased to maintain the original temperature. During the filling process the pressure in the 500 cm^3 reservoir drops by about 6 psi, corresponding to about 10^{22} deuterons.

The extruder chamber volume is 0.2 cm^3 and, if filled completely, would contain about .8 x 10^{22} deuterons. Thus, the filling efficiency of the extruder is about 80%. A complete fill is enough solid D_2 to make a 1 mm diameter extrusion 25 cm long.

The elements of the extruding system are shown in Fig. 4. In order to extrude a filament, two things are necessary: The solid D_2 must be raised to a temperature at which it will flow and pressure must be applied to force it out of the nozzle. Current is applied to the resistive heating element in the copper extruding head to raise the temperature of the D_2 to about $11^{o}K$, where it becomes plastic. A small motor is energized to turn a screw mechanism that moves the plunger in Fig. 4 downward to force the D_2 out the nozzle. The motor is energized manually and the progress of the extrusion is monitored by the operator on a closed circuit television screen.

A pellet is made by cutting the extrusion with two pairs of tungsten wires located directly below the extruding nozzle, as show schematically in Fig. 5 and in the photographs of Fig. 6. The shape of the extruded tip depends on when the last extrusion was made. To achieve uniformity in pellet shape, the filament is extruded to a length longer than necessary, and then cut to uniform length and shape by the lower, or trimming, pair of wires.

The pellet is then cut from the filament with the upper, or cutting, pair of wires. The cutting pair is located exactly one millimeter above the trimming pair.

Initially, the individual wires of a pair are two millimeters apart at the D_2 filament. The wires are initially curved and installed to lie in a plane perpendicular to the filament. In order to cut the filaments the wires are heated by passing 0.5 amp through each. The expansion of the curved wires, as a result of the Joule heating, causes them to move laterally inward until they are about 0.5 mm apart. If they are mounted without any stresses, the wires will remain in their original plane as they are heated. The kinematics of the wire motion is such that the wire moves about 75 μ toward the filament for each 10 μ of wire expansion. The cutting process is that of two hot wires moving into the deuterium filament from opposite sides, causing the filament to sublimate away in their immediate vicinity.

In order for the pellet to drop straight (It must drop 86 cm into a 1 mm diameter laser focal spot.) the frozen deuterium must attain a plastic state. The hot cutting wires cause the filament to sublimate until the pellet is hanging by a thread. The pellet must then shift its position without vibrating until its center of mass is exactly under the thread. If the thread breaks before the pellet shifts position or before it is motionless, the pellet will not drop straight. If the filament is too

cold, the thread will be brittle. The proper temperature is about $11^{o}K$. Higher freezing point gases, condensing on the filament, will also cause it to become brittle. Nitrogen is the only component of air that is troublesome. The other significant components of air are pumped by the liquid nitrogen shield. A vacuum system leak too small to register on an ionization gauge, but large enough to noticeably upset the normal H_2O to N_2 ratio on a mass spectrometer, will cause the filaments to become brittle. Figure 7 is a TV monitor screen photograph of a brittle filament caused by too low a temperature. Figure 8 contains photographs of properly plastic deuterium pellets just prior to dropping.

Figure 8 is typical of the uniformity of the pellets. The average pellet contains 1.9×10^{19} deuterium atoms with a standard deviation of 2.4×10^{18}. The last photograph of Fig. 8 shows the D_2 filament immediately after it was extruded. It is exactly 1.0 mm in diameter. This photo shows visually the amount of D_2 lost by sublimation during the pellet forming and dropping procedure. The atomic density of solid deuterium is 4.2×10^{22} cm^{-3} and the volume of a 1 mm x 1 mm right circular cylinder contains 3.3×10^{19} atoms. A little over a third of the pellet is lost before it drops.

The process of pellet making and dropping can be followed by watching the pressure in the chamber, which is shown as a function of time in Fig. 9. The pressure starts at 4×10^{-6} T

and rises as the extruder is warmed by the resistor in the extruding head. The filament is trimmed rather rapidly and the chamber pressure reaches its peak value during this part of the procedure. For the final cut, the cutting wire current is quickly brought up to 0.5 A and left at this value until the pellet drops, about 20 seconds later. The chamber pressure peaks again shortly after energizing the wires and drops to about 2×10^{-5} T as the pellet drops. The experimental background pressure is then 2×10^{-5} T.

Table I contains the vacuum system parameters and other numbers relevant to freezing D_2.

III. OPTICAL ALIGNMENT

The essential problem is to drop a 1 mm diameter solid deuterium pellet 86 cm into the 1 mm diameter focal spot of a Nd/Gl laser. Equally important is the detection of the pellet about one millisecond before it enters the focal spot, so that the laser can be fired at the instant of the pellet's arrival. Less stringent requirements are that the pellet be in the center of the vacuum chamber and cusp field, when it is irradiated, and that the resulting cloud be in the one centimeter diameter pulsed CO_2 laser beam. The reason that the pellet must be dropped so far is that the diamagnetic extruder must not be allowed to distort the cusp magnetic field.

Figure 10 is a schematic diagram of the pellet position detecting and trigger generating system. In order to mark the path of the falling pellet, a precisely vertical HeNe laser beam is established. This laser beam is oriented in the vertical direction to within 10^{-4} radians by reflecting the beam back on itself from a precisely horizontal glass plate. The part of the beam that is transmitted through the plate is colinear with the incident and reflected beams, and marks the path of the falling pellet. The horizontal glass plate is leveled with a machinist's precision level (L.S. Starrett Co. Master Precision Level No. 199) whose sensitivity is .0005 in/foot per small division of the bubble displacement.

After the plate has been leveled, the alignment is as follows: A HeNe laser that is nearly colinear with the Nd/Glass laser is aligned such that its beam exactly illuminates a burn pattern of the Nd/Gl laser on a polyethylene target that was moved into the center of the vacuum chamber for this purpose. The target is then removed and a three dimensional crosshair is positioned at the chamber center. Figure 11 is a photograph of the vacuum chamber interior showing the target and the crosshair. The vertical HeNe beam is then translated until it is centered on the crosshair. A set of prisms common to both the Nd/Gl laser and its associated HeNe laser are adjusted to center that HeNe beam on the crosshair. The image of the crosshair, illuminated by the HeNe beams, is then focused on the upper of two

slits in front of a photomultiplier tube. Finally the extruder is translated until its nozzle is centered in the vertical HeNe beam. The alignment of the plasma producing system is now complete.

The trigger signal that initiates the laser pulses as well as starting the timing sequence for the entire experiment is generated by the photomultiplier tube mentioned in the previous paragraph. The photocathode of the tube is masked by a plate with two slits, one 6.4 mm above the other. The upper slit is imaged on the center of the vacuum chamber by an f/6 set of optics. The lower slit is imaged 6.4 mm above the center. The vertical HeNe laser beam remains energized during the experiment, and light scattered from that beam into the lower slit generates a trigger signal 1.56 milliseconds before the pellet reaches the center of the chamber. The photomultiplier tube signal is fed into a nuclear instrumentation type pulse height discriminator to produce a timing pulse. Provided that there is no excess N_2 in the chamber, the vertical variation in the pellet position at the time of laser firing is less than $\pm$ 0.1 mm. Figure 12 includes a photograph, taken with an open shutter camera, of a pellet falling in the vertical laser beam.

This concludes the description of the alignment process for the generation of plasma from falling pellets. It does not include the necessary procedures associated with the laser scattering and interferometric diagnostics.

IV. PLASMA GENERATION

The frozen D_2 pellet is ionized by a two laser process. A $\sim$ 100 J pulse from a Nd/Gl laser[9] first evaporates the pellet, forming a cloud that expands in a vacuum. A $\sim$ 1000 J CO_2 laser[10] pulse ionizes this cloud by a laser spark process. The result is a plasma of 2×10^{19} ions at an energy of $\sim$ 40 eV. The reason for the two laser process is that the pellet is too large to be ionized by a single laser pulse, unless it would have an extremely long duration. There are two reasons for generating such a large plasma: First, an original goal of this project was to develop a plasma source for an experiment that required a plasma of $10^{20} - 10^{21}$ ions. Second, the large plasma insures, for ease of spatial resolution, that the scale length of the plasma size is at least an order of magnitude larger than the ion Larmor radius which is of the order of a centimeter.

The accepted theory for the generation of plasma from solid targets by laser irradiation is that of Puell.[11] This theory is valid for laser pulses longer than a nanosecond and for laser intensities that are low enough to permit electron-ion thermalization of plasma as it is being generated. According to this theory, in order to completely ionize a one millimeter cube of solid hydrogen with a 1000 Joule CO_2 laser pulse, a pulse duration of 30 μsec would be required. Thirty microseconds amounts to a steady state plasma source on the anticipated time

scale of this experiment. Such a source may well be interesting but it would not lead to the rapid filling of a cusp magnetic field. The plasma generation scheme described below, creates plasma with an initial volume of 1.0 cm^3 during the 70 nsec spike of the CO_2 laser pulse.

When the deuterium pellet containing 2×10^{19} atoms reaches the center of the magnetic cusp field, it is irradiated by a 100 Joule, 40 nsec, Nd/Gl laser pulse. See Fig.13. This energy ionizes the incident side of the pellet, producing a plasma of about 10^{18} ions at a temperature of about 100 eV. This plasma rapidly "blows off" setting up sufficient shock waves in the solid pellet to vaporize it. Since only .02 Joules is required to vaporize a one millimeter cube of D_2, there is a lot of room for optimizing this part of the process. Figure 14 is a Schlieren study of the expansion of the D_2 cloud. The cloud expands at a 1.7×10^5 cm/sec rate which corresponds to a temperature of $300^{\circ}K$ or $600^{\circ}K$, depending on whether the velocity is applied to deuterium atoms or molecules. The pellet is completely vaporized.Schlieren photographs taken at 6 μsec after the Nd/Gl laser pulse are perfectly clear, indicating no particulate matter above a 25 micron size. The expansion velocity that is measured from Schlieren records, which record density gradients rather than density, must be considered a lower limit. The shadowgraph edge is not tied to the particles, but

must recede inward relative to the flowing particles as the particle density decreases.

The cloud is allowed to expand for two microseconds, to a radius of at least .34 cm or a corresponding density of at most $.9 \times 10^{20}$ cm^{-3}. This density is ten times the critical density for 10.6 μ radiation if the cloud were fully ionized. If it is allowed that the expansion velocity is 50% higher than indicated by the Schlieren records, the cloud density would be a factor of three lower than $.9 \times 10^{20}$ cm^{-3}.

Two microseconds after the Nd/Gl laser pulse, the cloud is ionized and heated by a 1000-1500 Joule pulse from a CO_2 laser. The pulse consists of a 70 nsec duration initial spike that contains 30% of the pulse energy and a 1.5 μsec tail that contains the rest. It is the initial spike that interacts with the D_2 cloud. At the expansion rate of the ionized cloud, the plasma density during the laser pulse tail is too low for any interaction to occur. The CO_2 laser pulse completely ionizes the D_2 cloud and heats it to an expansion velocity of $.7 \times 10^7$ cm/sec. By trial and error, it was determined that the combination of a 2 μsec delay between laser pulses and defocussing the CO_2 laser to a 1 cm diameter spot size at the cloud resulted in complete ionization of the D_2. Combinations of smaller spot size and shorter time delays did not effectively ionize the cloud. Larger spot diameters and longer delays

were not investigated. In the experiments described hereafter, the D_2 cloud was positioned 6 cm beyond the focal point of a 1.0 meter focal length, f/4.5, salt lens. For a 1200 Joule laser pulse, the peak intensity of the 10.6 μ radiation at the cloud is 7.0×10^9 watts/cm^2 and the beam diameter at half intensity is 1.0 cm.

Figure 15 is a holographic interferogram of the expanding plasma, taken 0.4 μsec after the initial spike of the CO_2 laser. Inversion of the fringe pattern indicates over 10^{19} electrons and leads to the conclusion that the plasma is fully ionized. Also evident from Fig. 14 is that the plasma is slightly asymetrical, tending to blow off toward the CO_2 laser.

The further properties of this plasma, that is to be used to fill a magnetic cusp, are measured with Langmuir probes and spectroscopically. Figure 16a shows the Langmuir probe trace produced by the plasma and compares it to a Maxwellian plasma with an ion thermal velocity of $.66 \times 10^7$ cm/sec containing 2×10^{19} ions. The probe has an area of 1 mm^2 and is located 30 cm from the plasma center, in the plane of the ring cusp. In accordance with the interferogram, the probe would have indicated a higher current had it been located to detect plasma expanding toward the CO_2 laser, and vice versa.

Figure 16b shows the spectrum of the visible radiation emitted by the plasma. Although the system is sensitive enough

to record hydrogen lines out to radial positions of 5 cm, there is no indication at any position of any impurity line radiation.

The summary of the plasma production is as follows: A fully ionized single ion species D^+ plasma containing $> 10^{19}$ ions is produced. The plasma is spectroscopically pure and has an average expansion velocity of $.7 \times 10^7$ cm/sec. The plasma is created in an initial volume of about one cm^3. It therefore contains no wall-connected field lines or currents. The only magnetic field lines through the plasma should be those present in the volume when the plasma is created. This plasma is ideal for filling a cusp with a $\beta = 1$ plasma of known properties.

V. THE MAGNETIC CUSP EXPERIMENT

The principal loss mechanism of plasma from a magnetic cusp configuration is leakage of the plasma through the cusps to the chamber walls. The lifetime of the confined plasma is, therefore, inversely proportional to the area of the plasma at the cusps. In the case of the ring cusp, its area is just the product of 2π times the plasma radius times the width of the cusp. The goal of the present experiment, after creating the plasma in the center of the magnetic cusp configuration, is to show that the plasma is confined by the magnetic field, and then measure the width of the ring cusp and correlate this width with the observed plasma lifetime. The cusp width must then be

related to gyroradii or the plasma particles in order to correlate this experiment with previous work and theory. The advantages of the present experiment over previous experiments are 1) that the plasma is free of the magnetic field and contains a single ion species, and 2) the method of measuring the cusp width by laser scattering techniques avoids the possibility that the measurment affects the result. Figure 17 is a schematic diagram of the experiment that shows the laser scattering system.

In order to show that the plasma is confined by the cusp magnetic field, open shutter and streak pictures of the chamber walls were taken. Figure 18a is an open shutter photograph of the interior of the vacuum chamber that shows the radiation emitted from the walls during the experiment. The ring of light is located at the ring cusp and is generated by escaping plasma. The width of this ring is about one centimeter, the same as the ring of chemical etching or deposit around the wall. Figure 18b is a photograph of the wall light emitted at a chamber window. Figure 18c is a streak photograph of this light. This streak photograph shows the wall light reaching a peak intensity about 3 μsec after the ionization of the plasma and then decaying over the next 7 μsec. The emitted light in this streak photograph shows very little azimuthal variation.

A qualitative measurement of the point cusp losses was made by placing an epoxy-fiber-glass plate at a point cusp location. The intensity of the radiation from the plate caused by plasma

impact, and the size of the radiating area, indicates that point cusp losses are much smaller than ring cusp losses.

The plasma is created at the center of the cusp configured magnetic field, where the field is zero, and expands radially against the linearly increasing magnetic field. See Appendix I. As the plasma expands it pushes the magnetic field ahead of itself, completely excluding ($\beta > .99$) the field from its interior. The position of the plasma-magnetic field interface, as a function of time, is recorded on a shot-to-shot basis by a radially movable magnetic probe. Since the plasma expansion is on a much shorter time scale than the 60 μsec risetime of the cusp field, magnetic flux through the field coils is conserved during the expansion process. This is confirmed by the magnetic probe signals which show the magnetic field rising as flux is compressed between the plasma and the coils, and then dropping to zero as the interface passes over the probe. The plasma radial extent reaches a maximum and then the magnetic field collapses and is restored to its original value. The result of these magnetic probe measurements, taken at different radial positions on subsequent shots is shown in Fig. 19. Along a radial line located 27° from the ring cusp, the plasma expands at a velocity of 0.7×10^7 cm/sec. It reaches a maximum radius of 15 cm in about 2.2 μsec and then collapses, at a rate almost equal to its expansion rate. There is no plasma "bounce." After 6 μsec the $\beta = 1$ phase of the experiment, which is the phase that is interesting,

is over. The 6 μsec lifetime of the $\beta = 1$ plasma correlates very well with the time history of the emission of visible light at the ring cusp. It remains now to measure the plasma density distribution across the ring cusp to quantify the losses.

The Thomson scattering diagnostic system that is used to determine the spatial distribution of the plasma electron density at the ring cusp is shown in Fig. 20. Not shown in the figure is the scattering laser, a 0.25 J Korad ruby laser with a 20 nsec pulse width. The laser pulse passes through the plasma along an optic axis that is parallel to, and 22 cm above, the cusp symmetry axis. The 0.6 cm diameter laser beam is focussed on the ring cusp with a 1.0 m focal length lens, producing a one millimeter diameter focal region that extends perpendicularly across the ring cusp.

The ruby light that is scattered by the electrons in the focal volume is ultimately imaged on a linear array of four fiber optic bundles, each of which is coupled to its own photomultiplier tube. The array of fiber ends consists of one millimeter wide bundles separated by 0.25 mm. The imaging optics are shown in Fig. 20. The fiber bundle array is located at the exit slit of a 0.5 meter Spex monochromator, and is oriented such that the four bundles are imaged, through the monochromator, along the entrance slit. In this case the monochromator is used only as a wavelength filter. The ruby laser focal volume is also imaged on the entrance slit of the monochromator, along its optic

axis. Since the ruby laser focal volume is a horizontal cylinder and the entrance slit is vertical, the optical train contains a 90^{o} image rotator. The detection system is aligned on the plasma by adjusting the periscope mirrors. The imaging optics from the ruby laser focal volume to the entrance slit reduce the image size by a factor of four. This means that four 0.4 cm long segments of plasma volume, separated by 0.1 cm, are each imaged on a separate PM tube. The four segments are located symmetrically across the ring cusp.

The system is calibrated and aligned using Rayleigh scattering from N_2 at a pressure of .01 atm, which corresponds to an electron density of 0.7×10^{15} cm^{-3}. An optical fiber bundle directly linking the ruby laser and the monochromator exit slit provides a fiducial mark for determining the time of arrival of the scattering signal.

The experiment consists of generating the cusp plasma and measuring the instantaneous plasma electron density across the ring cusp at various intervals after the CO_2 laser fires. The results are shown in Fig. 21, and some individual oscilloscope traces of the scattering signal are shown in Fig. 22. Each point of Fig. 21 is an average of two to four shots. From this figure, it is evident that the width of the cusp (full width, half maximum) is very close to one centimeter and does not change appreciably with time.

The detection system is converted to measuring wavelength dispersion rather than spatial variation, by rotating the fiber optic array at the monochromator exit by 90^{o}. With this change installed, the wavelength dispersion of the scattered light is measured, and a plasma electron temperature is inferred. The result is shown in Fig. 23. The electron temperature that best describes the plasma is about 15 eV.

The data of Fig. 23 were taken at 3 and 5 μsec after the CO_2 laser had fired. A sudden drop in temperature, as might result from an influx of cold plasma from the walls, was looked for at later times, but not found. Also, attempts were made to observe plasma rotation, by measuring the spatial variation of the scattered light at different monochromator wavelength settings, and looking for a Doppler shift. No rotation was observed.

The conclusion of the laser scattering experiment is that the wall light and wall chemical deposits give a true indication of the width of the ring cusp, viz. about one centimeter.

VI. DISCUSSION OF RESULTS

The immediate question to be discussed is "What is the scale length of width of the ring cusp?", and the answer is that all of our measurements indicate that it is of the order of the ion Larmor radius. The laser scattering result, Fig.

21, and the vacuum chamber wall chemical deposits and light emission, Fig. 18, show the cusp width to be very near one centimeter. The expansion velocity of the plasma, Fig. 19, is 0.7×10^7 cm/sec, which corresponds to a deuteron energy of 50 eV. The vacuum magnetic field at the position where the laser scattering measurements are made (z = 0, r =22 cm) is 1.7 kGauss. Since the ions cool as they expand, all of the ion energy is in kinetic energy of expansion, and 50 eV is the total ion energy. The ion energy in circular motion around field lines is always less than this amount. From these values, the upper limit of the ion Larmor radius is computed to be 0.9 cm. At the intersection of the ring cusp and the chamber wall the vacuum field is 2.1 kGauss and the ion Larmor radius, there, is computed to be at most 0.7 cm. These values are to be compared with the electron Larmor radius. The electron temperature is measured to be 15 eV, Fig. 23, and the electron Larmor radius that corresponds to this temperature and the vacuum magnetic fields, as mentioned above, is between .0065 and .0080 cm. This value is two orders of magnitude below the measured cusp width. The hybrid Lamor radius, which is the geometric mean between the ion and electron radii, is between .07 and .08 cm; one order of magnitude smaller than the measured cusp width. Thus it is concluded that the width of the ring cusp is of the order of the ion Larmor radius.

The laser scattering cusp width measurement is particularly significant because it does not interfere with the evolution of

the plasma. On the other hand, the laser scattering system detects the total number of electrons in each of four tandem volume elements 0.4 cm long and separated by 0.1 cm. The question arises as to whether this resolution is good enough to rule out the possible conclusion that the cusp width is, say, two hybrid radii in width, or .2 cm. The structure of the cusp density profile is not known, but suppose it is Lorentzian, with a full-width-half-maximum length of 0.2 cm: $n(z) = (10/\pi)(1 + (10z)^2)^{-1}$. The result of a measurement of this density distribution by the laser scattering system is that over 84% of the detected electrons fall into one or two channels and the "outside" channels receive signals that are less than one tenth of the signals received by the "inner" channels. The results of Figure 21, then, rule out the possibility that the cusp width is actually very narrow but that the narrowness was masked by the resolution of the apparatus.

In a meaningful experiment in measuring the ring cusp width, the resistive skin depth must be small compared to the measured width. The resistive skin depth, in MKS units, is given by the equation

$$L^2 T^{-1} = \left(\frac{\mu_o \sigma}{2}\right)^{-1} ,$$

where L is the skin depth, T is the ion transit time out of the magnetic well ($T = R/v_i$), μ_o is the free space permittivity,

and σ is the plasma conductivity. This result is due to R.J. Bickerton. In the present experiment, the ratio of L to R_{Li} is 0.38 where σ is computed for a 15 eV electron temperature plasma and T, the ion transit time, is 3 μsec. (The cusp width is measured at R = 22 cm and v_i is 0.7×10^7 cm/sec.) During the plasma expansion, the sheath is being compressed as the plasma expands into higher magnetic field regions. Also, as the plasma expands, the sheath is being azimuthally stretched. These two effects reduce the sheath thickness, during expansion, by a factor of $1/\sqrt{5}$. Although L is not negligible, it is small compared with R_{Li}. Table II shows the skin depth ratios of previous experiments. With the exception of Sekiguchi's 100 eV plasma, the ratio in all the high β experiments was about 0.3 - 0.4. Bickerton's calculation assumed a stationary plasma boundary that reached an equilibrium thickness where plasma loss along field lines balances plasma diffusion across lines. It is not clear how applicable this model is to our dynamic case of an expanding and collapsing plasma. At any rate, the effect of magnetic field diffusion due to plasma resistivity is as small in this experiment as it was in all except one past experiment.[3]

The lifetime of the high beta plasma in the magnetic cusp is related to the cusp width by an effusion formula:

$$N = C\int_0^{\tau} 2\pi R\delta v_i n dt \qquad (1)$$

where N is the total number of ions in the plasma, R is the cusp radius (R = 22 cm), δ is the width of the cusp, n is the ion density at the ring cusp, and v_i is the ion velocity. The constant accounts for losses out of the point cusps (which we believe to be small compared to the ring cusp losses) and for the particles whose velocities are not exactly radial as they enter the ring cusp. (For an isotropic distribution and no point cusp losses C = 0.25.) Most of the plasma particles can be accounted for as leaving the ring cusp if it is assumed that the ion velocity is radial and that the velocity at time t and position R is R/t. Setting C equal to one, v equal to R/t, R equal to 22 cm (The radius corresponding to the laser scattering.), and using the densities and cusp width from Figure 21, the integral of equation (1) from 2.5 μsec to 12.5 μsec results in a total of 10^{19} ions; or about half of the plasma. This number is reasonable since some of the plasma is lost through the point cusps and some recombines as it expands and cools adiabatically.

Finally, then, the result of the experiment can be stated as follows: A pure, high β plasma, created at the center of a cusp magnetic field, expands radially, pushing the magnetic field outward, and streams out of the ring cusp, which is about an ion Larmor radius wide. The appropriate streaming velocity is near the self similar expansion velocity (v(R,t) = R/t). The plasma reaches a maximum extent and then collapses, ending

the high β phase of the experiment. The lifetime of this high β is less than a factor of two larger than the free expansion lifetime of the plasma without the magnetic field.

VII. ACKNOWLEDGEMENTS

The authors wish to acknowledge the continued interest and support of Dr. A.E. Robson during the course of this research. We also wish to thank Dr. William Friedman of the Laboratory for Laser Energetics, University of Rochester, for the use of, and the instruction in the use of, his deuterium extruder. Two of us (JRG and REP) also wish to acknowledge some very useful discussions with the late Dr. W. Riedmuller of the Institute for Plasma Physics, Garching, on the cutting of deuterium filaments. We also wish to thank Mr. Edward Laikin and Mr. James Cheadle for their technical assistance, and Mr. Sam Rod for his mechanical design.

References

1. Spalding, I., Advances in Plasma Physics, 4, (Simons, A., and Thompson, W.B., Editors) John Wiley, New York (1971).

2. Haines, M.G., Nuclear Fusion 17, 4, page 811 (1977).

3. T.K. Allen and I.J. Spalding, Phys. Fluids 8, 2032 (1965).

4. A. Kitsunezaki, M. Tanimoto, and T. Sekiguchi, Phys. Fluids 17, 1895 (1974).

5. Hershkowitz, N. Leung, K.N., and Romesser, T. Phys. Rev. Lett. 35, 277 (1975).

6. Kogoshi, S., Sato, K.N., and Sekiguchi, T., J. Phys. D: Appl. Phys. 11, 1057 (1978).

7. H. Baumhacker, H. Brinkschulte, R.S. Lang, W. Riedmuller, and M. Salvat, Applied Physics Letters 30, 461 (1977).

8. W.D. Friedman, G.M. Halpern, and B.A. Brinker, Rev. Sci. Instr. 45, 1245 (1976).

9. J.R. Greig and R.E. Pechacek, "A 100J, 40-nsec Q-Switched Nd/Glass Laser", NRL Memorandum Report 3461, Naval Research Laboratory, Washington, DC.

10. R.E. Pechacek, J.R. Greig, M. Raleigh, and Sam Rod, "The NRL One Kilojoule CO_2 Laser," NRL Memorandum Report 3602, Naval Research Laboratory, Washington, DC.

11. H. Puell, Z. Naturforsch, 25a, 1807 (1970).

12. W.A. Perkins and C.J. Brown, J. Appl. Phys. 35, 3337 (1964).

Table I

Pellet Size: 1 mm diameter by 1 mm long

Number of deuterium atoms in pellet: $(1.9 \pm .24) \times 10^{19}$

Cutting wires: 100μ diameter tungsten wire

Wire current: 0.5 amp

Wire temperature: $\sim$ 800° F

Vacuum chamber size: 500 liters

Vacuum pump: 800 liter/sec
Turbomolecular pump

Table II

Exp't	Measured Cusp Width	Te (ev)	$T(10^{-6}$ sec)	L(cm)	R_{Li}(cm)	L/R_{Li}
Allen, et al., 1966	$\sim R_{Li}$	70	1.	.059	(.068?)	.5-.3
Kitsunezaki, et al., 1974	$\sqrt{R_{Li}R_{Le}}$ R_{Le}	30 100	.6 .33	.123 .037	.34 .61	.36 .083
Hershkowitz, et al., 1975	$\sqrt{R_{Li}\ R_{Le}}$	3	37.	3.85	1.41	2.73
Kogoshi, et al., 1978	$\sim R_{Li}$	50	.42	.049	.160	.31
Pechacek, et al., 1979	$\sim R_{Li}$	15	3	.33	.88	0.38

Appendix I

The Cusp Magnetic Field

The cusp configured magnetic field is generated by a pair of single turn coils, 71 cm in diameter and axially separated by 65 cm. The coils are driven by a 0.5 MJ capacitor bank consisting of 32 modules of six 14 μf, 20 kv capacitors. Each module is switched by a trigatron spark gap. The circuit is damped by a set of varistors. The current risetime is 60 μsec.

The curves of Figs. 24 to 26 were plotted using numbers generated by the MAFCO[12] magnetic field calculating code. Figure 24 shows the field line curvature in one quadrant of a plane through the cusp symmetry axis, and the axis of the magnetic probe that is used to detect the plasma expansion. Figure 25 shows the magnetic field parallel and perpendicular to the probe axis as a function of probe position. The values are those corresponding to the peak of the coil current. Figure 26 is a plot of the fields through the cusps.

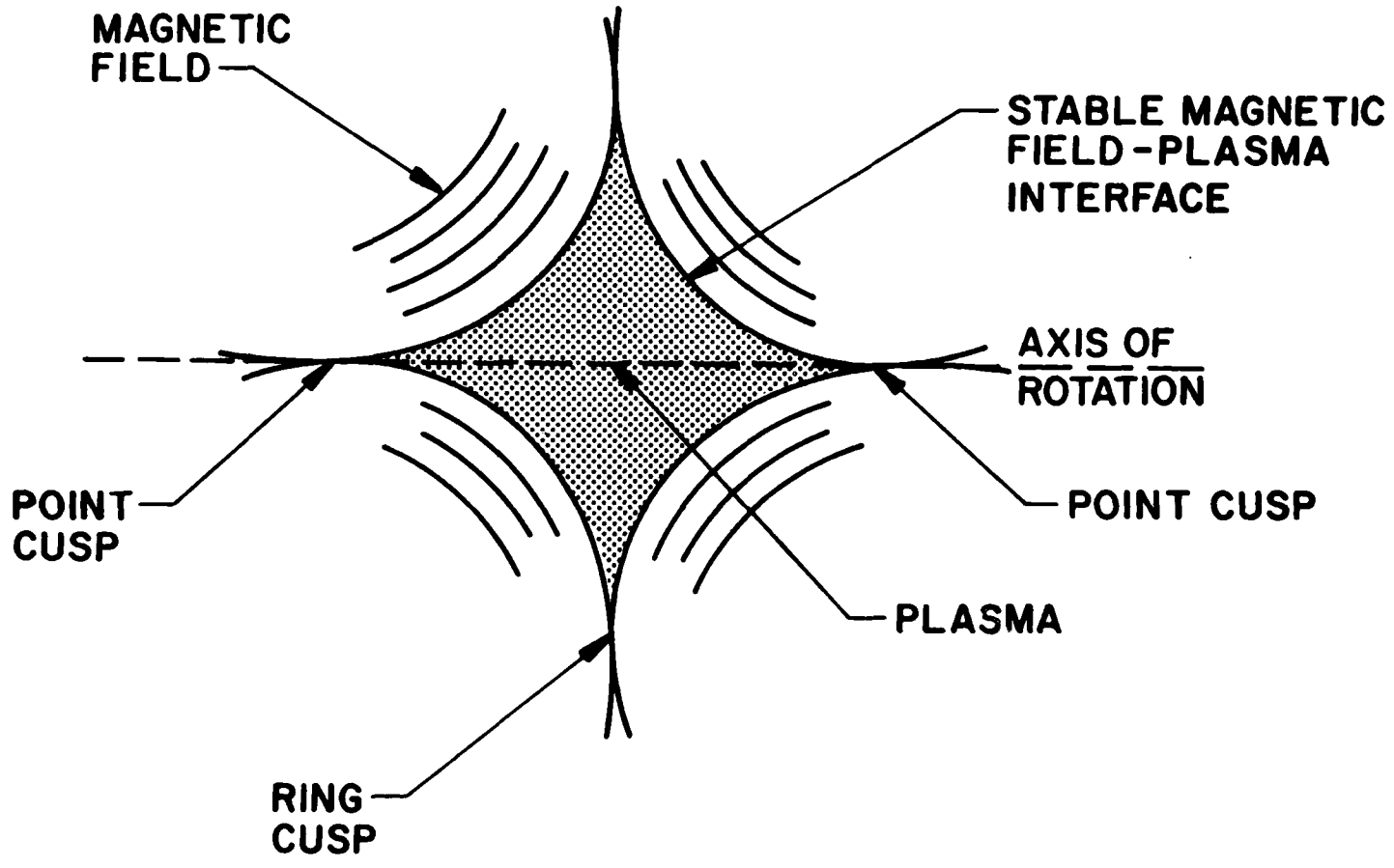

Fig. 1 — Diagram of a plasma contained in a cusp magnetic field. Note that the plasma-magnetic field interface is everywhere convex toward the plasma, and that plasma can leak out of the point and ring cusps.

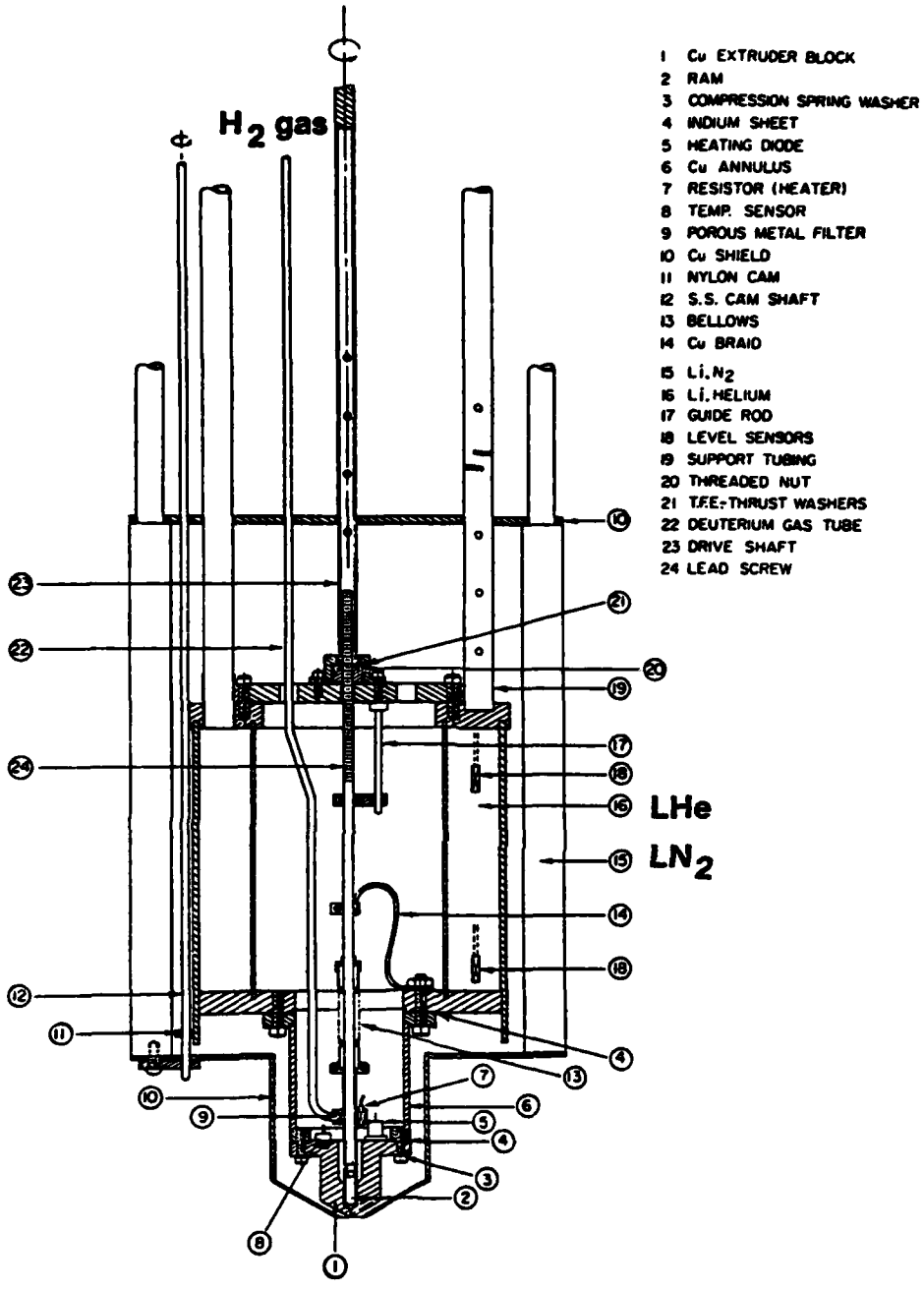

Fig. 2 — Mechanical drawing of the University of Rochester deuterium extruder which is used in the pellet dropping system.

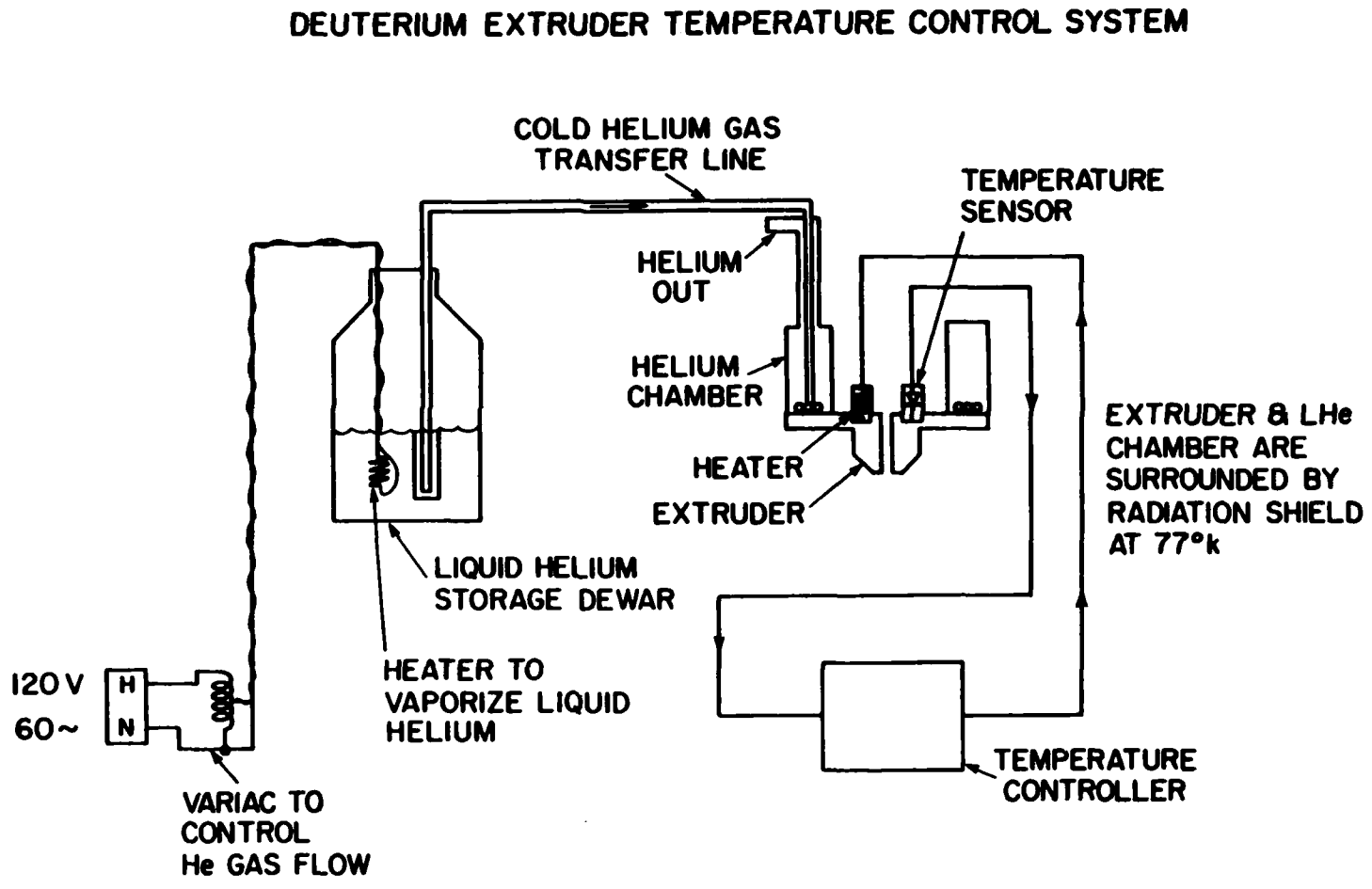

Fig. 3 — Schematic diagram of the deuterium extruder temperature control system. Coarse control is maintained by the rate of evaporation of helium in the storage dewar. Fine control is provided by an electronic temperature controller and a resistance heater.

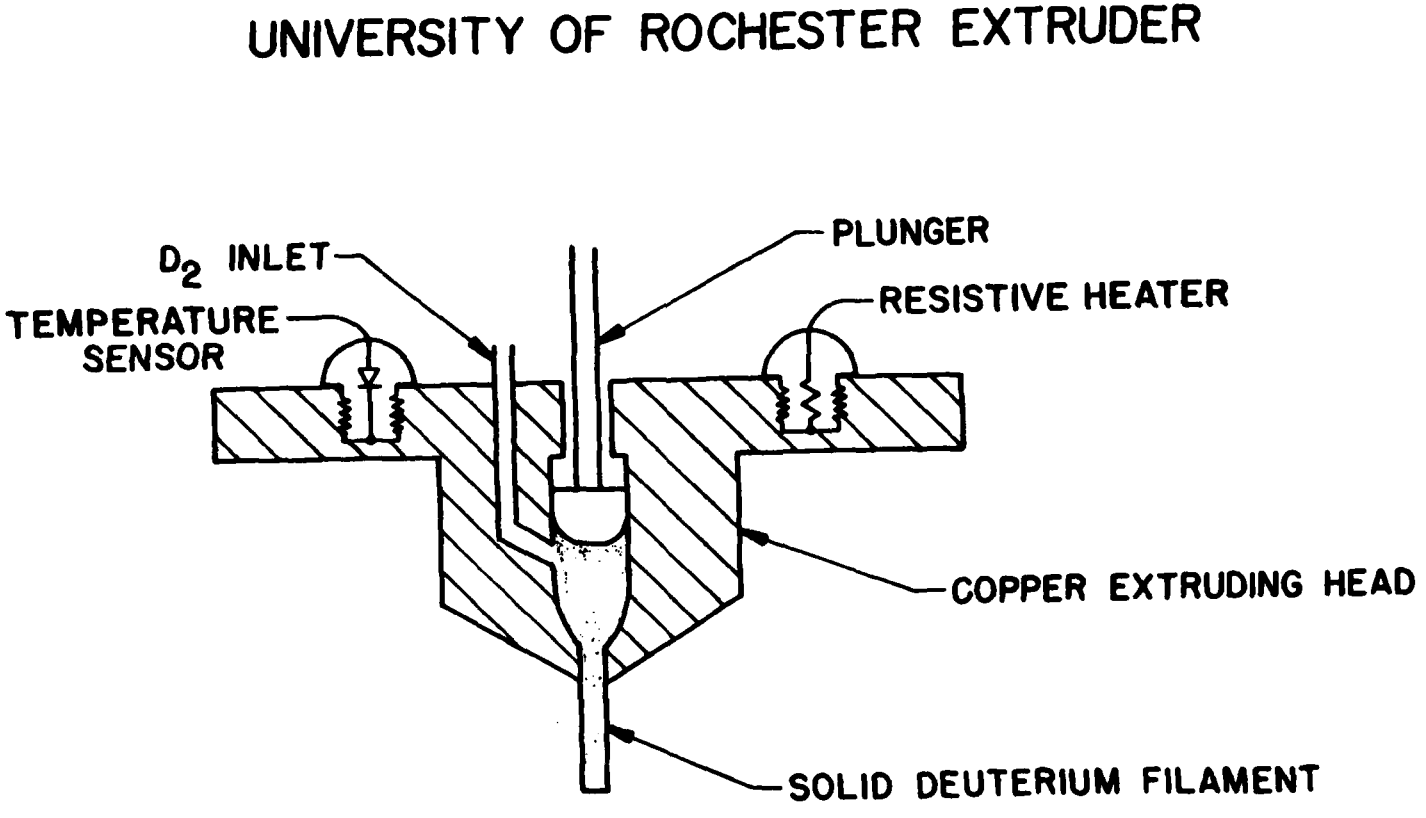

Fig. 4 — Schematic diagram of the deuterium extruder head.

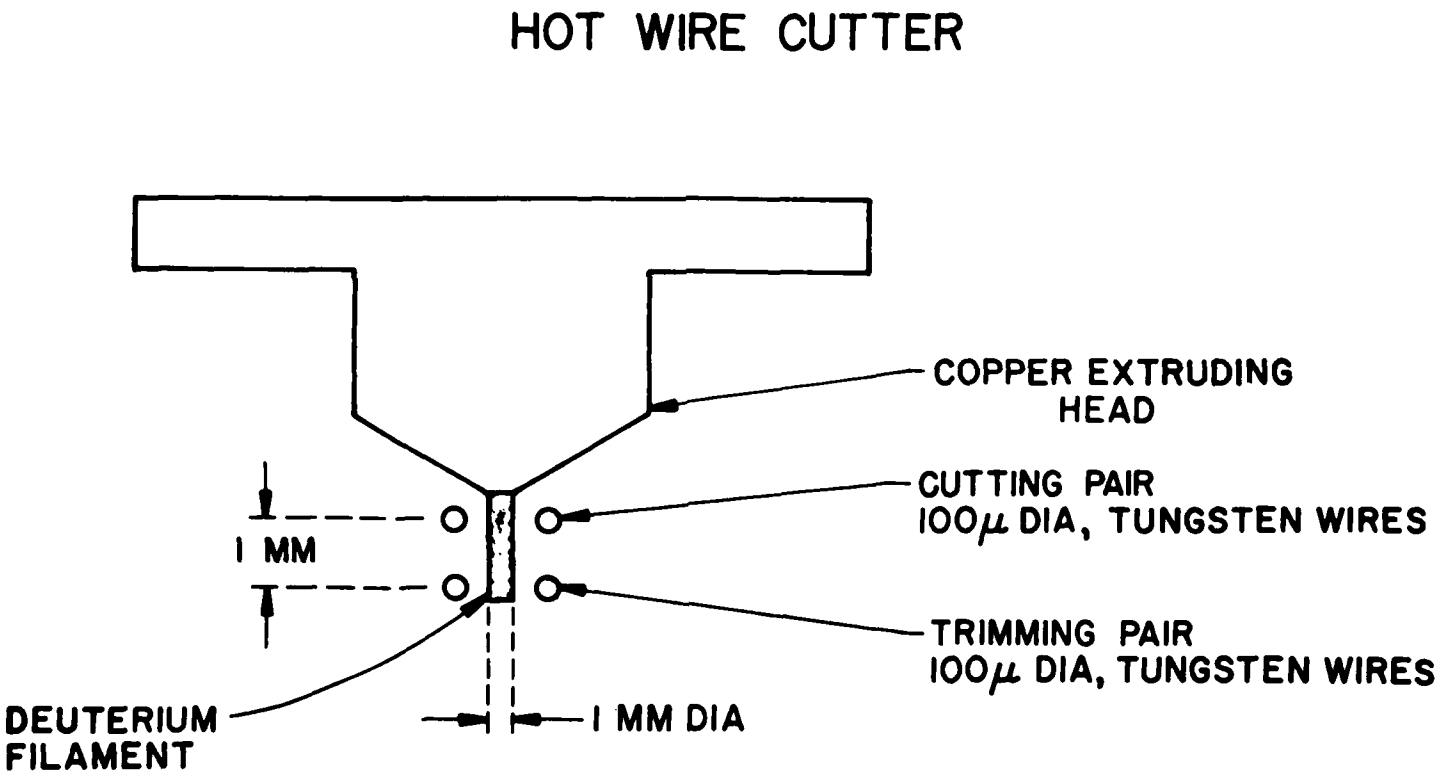

Fig. 5 — Schemataic diagram of the deuterium filament cutting system.

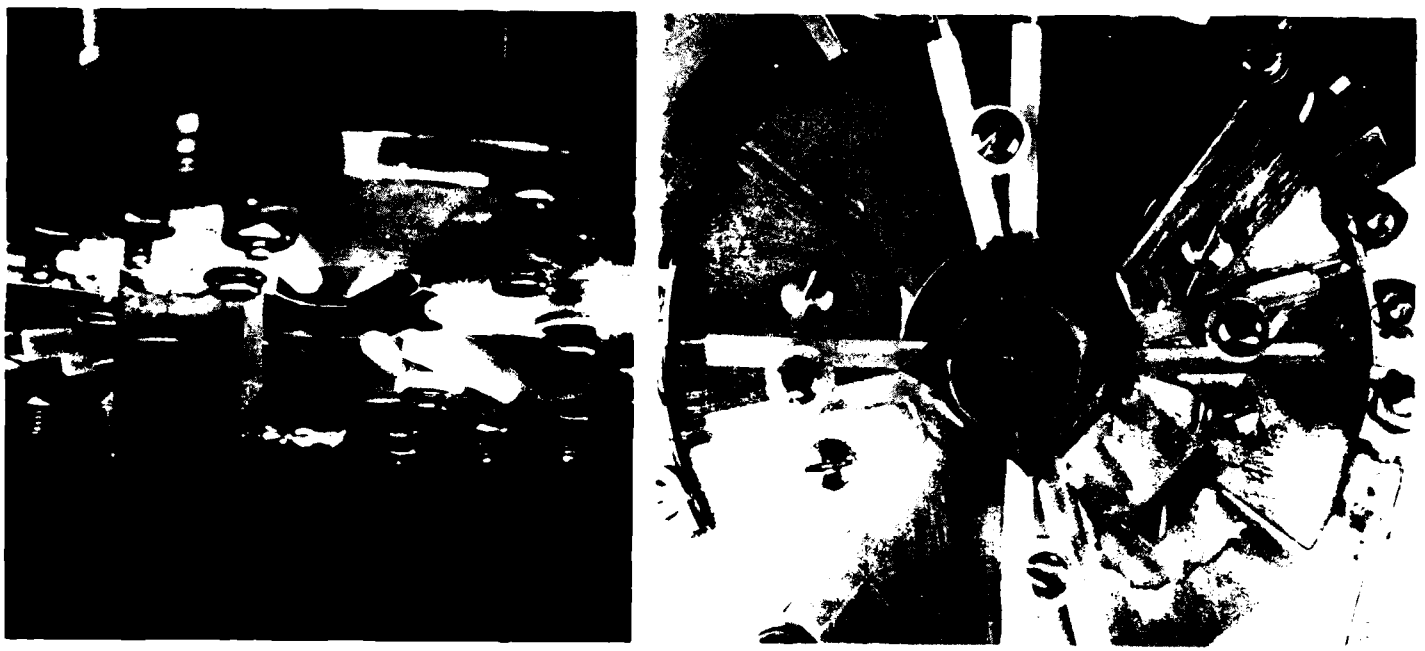

Fig. 6 — Photographs of the extruder nozzle and cutting wires. Figure (a) shows the two prism periscope through which closed circuit TV observations are made.

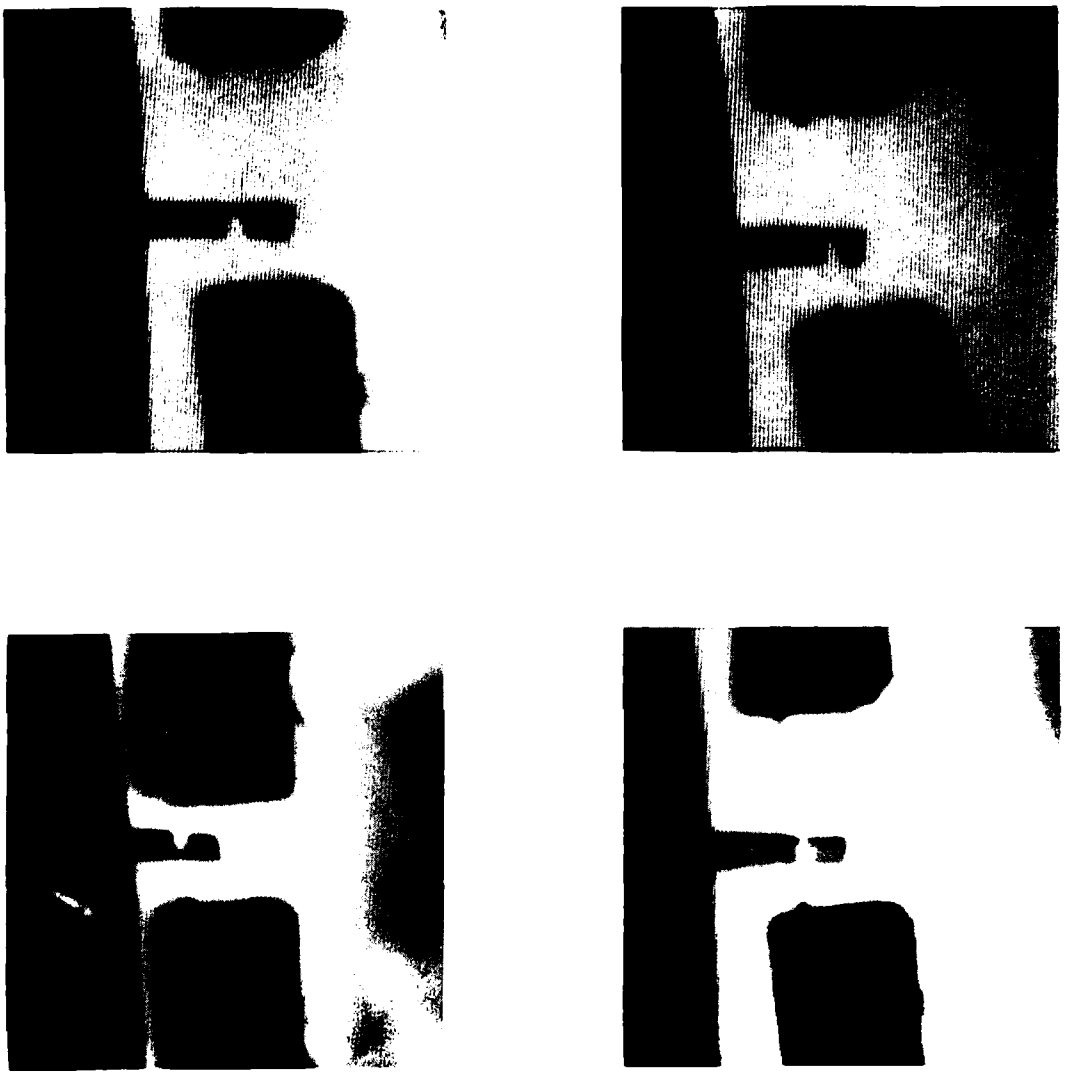

Fig. 7 — Photographs of TV screen image of very cold filaments (T ~ 4.2° K). The photographs illustrate the brittleness of the material.

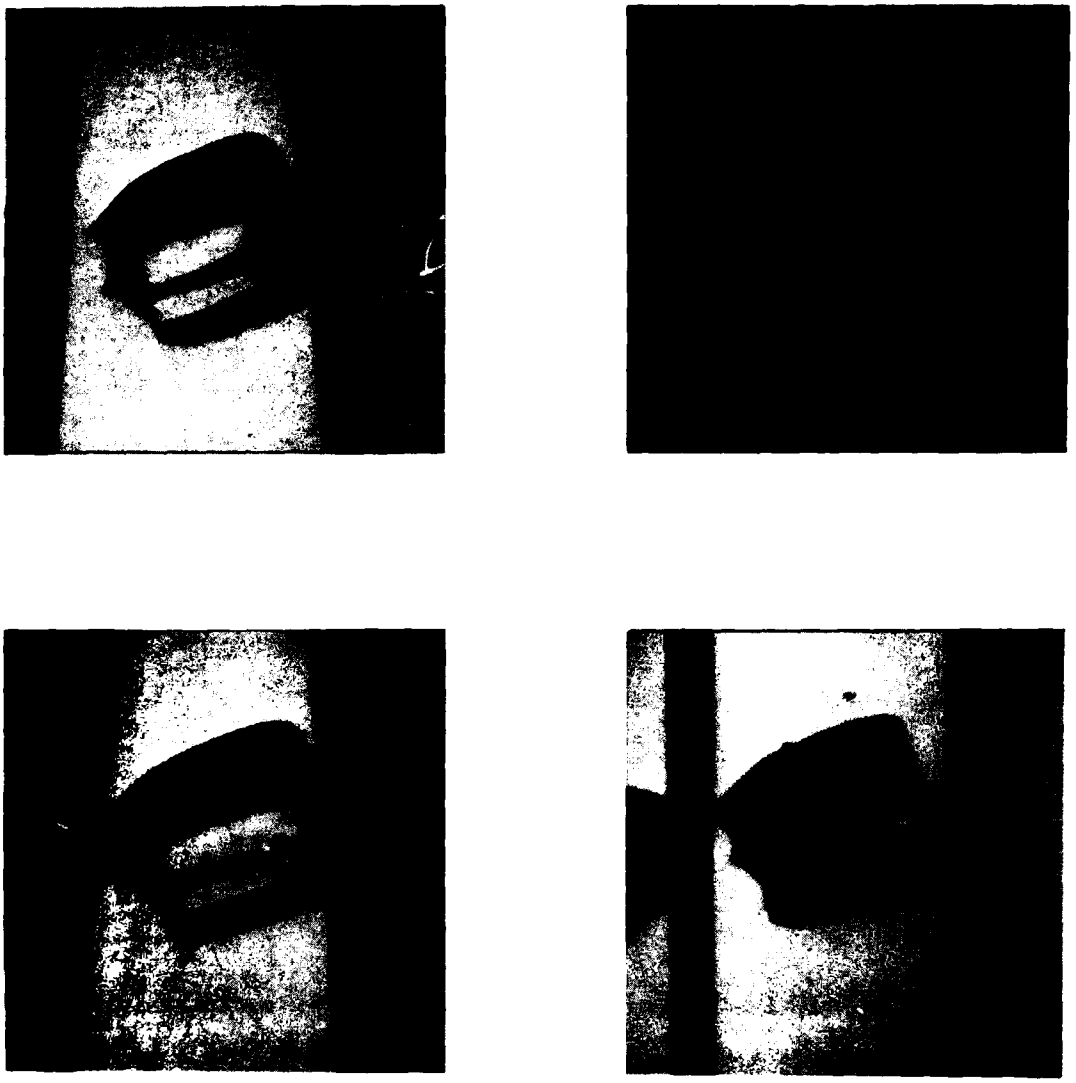

Fig. 8 — Photographs of TV screen images of deuterium filaments. The cutting and trimming wires are shown. In figures a, b, and c the filament has been trimmed and the pellet is ready to drop. Figure d shows the uncut filament, 1 mm in diameter before it has been reduced in size by evaporation.

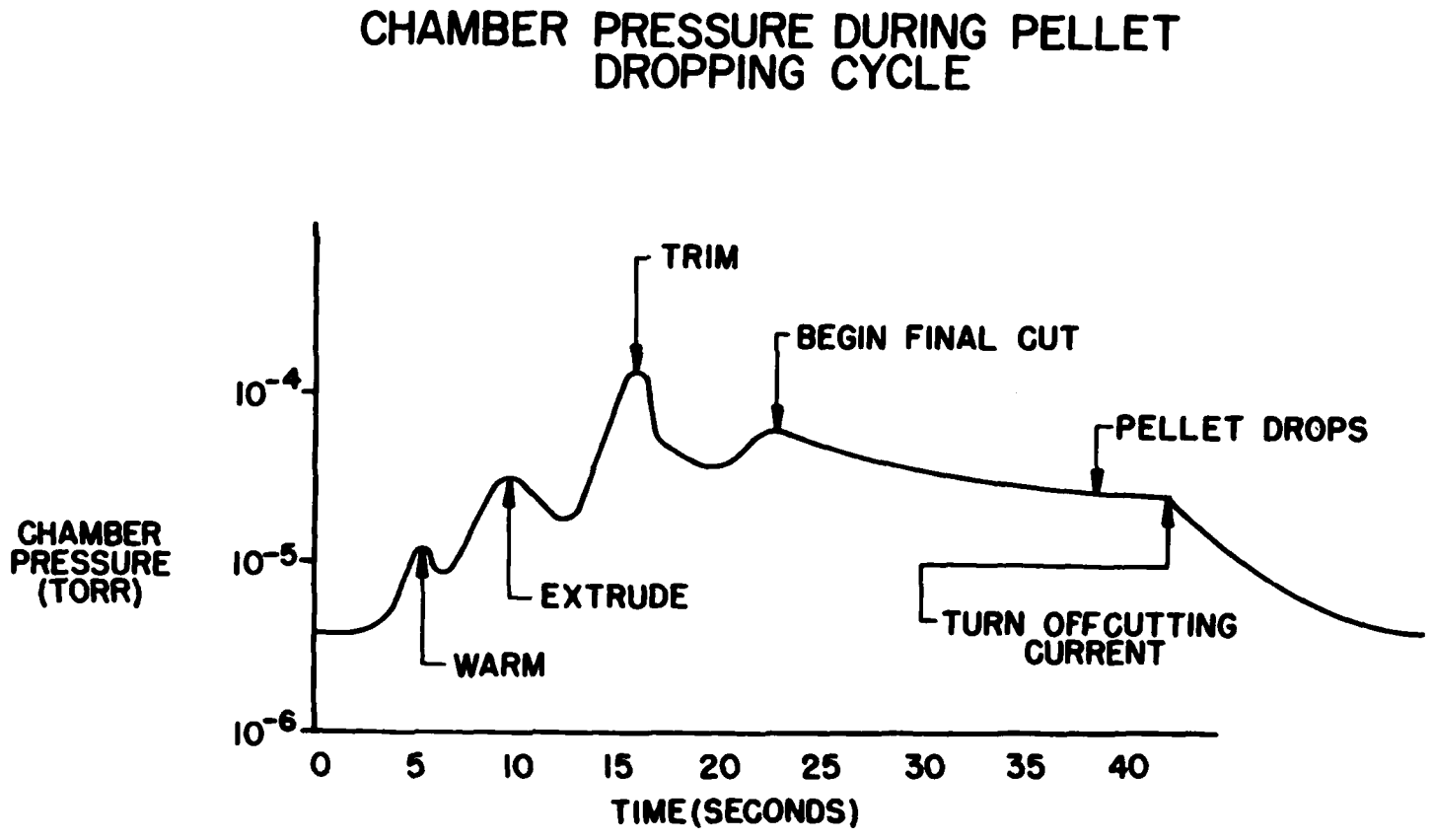

Fig. 9 — Plot of vacuum chamber pressure versus time during the deuterium extruding and cutting process.

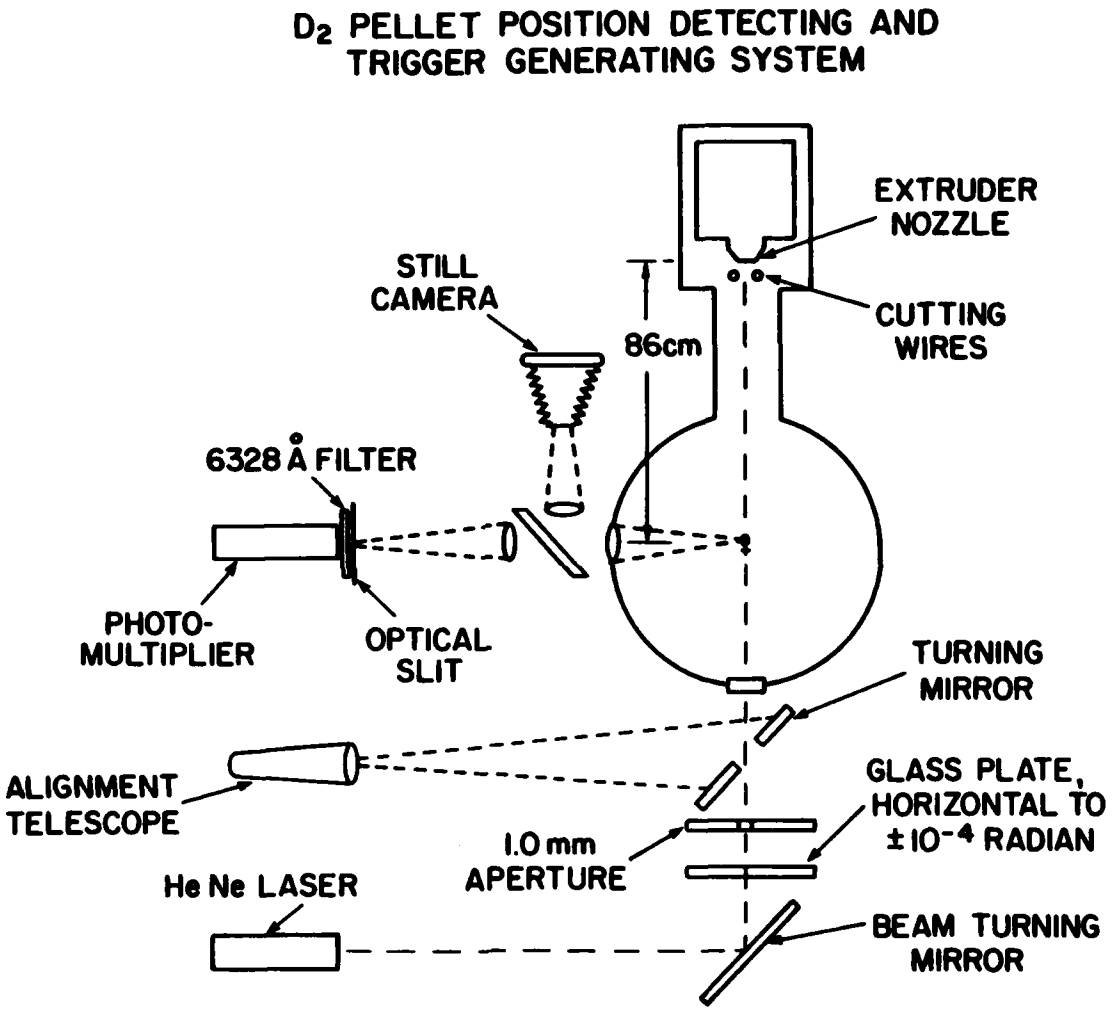

Fig. 10 — Schematic diagram of the optical system used to position the extruder and to detect the position of the falling pellet and generate a master trigger signal.

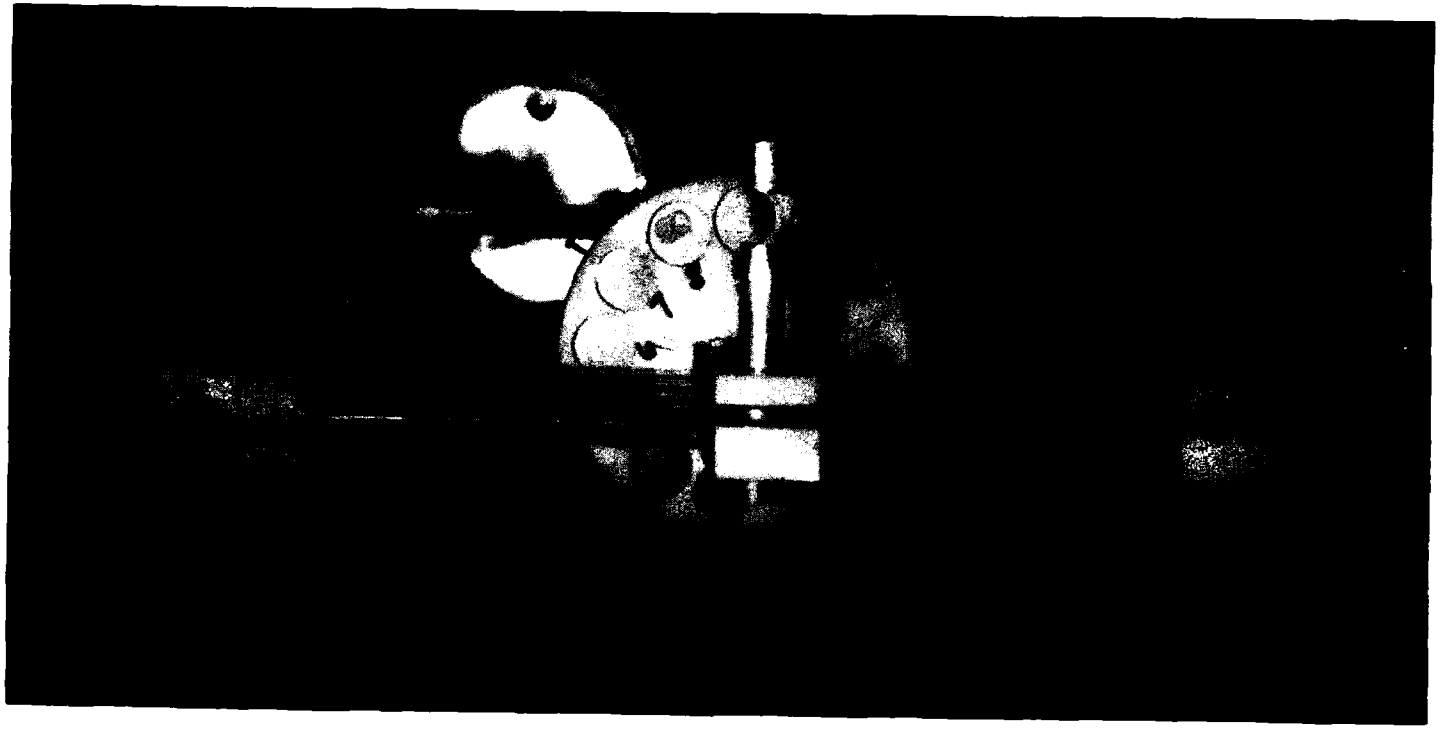

Fig. 11 — Photographs of the interior of the CUSP vacuum chamber showing the laser alignment target and the three dimensional alignment crosshair.

VAPORIZATION OF A FREELY FALLING D_2 PELLET

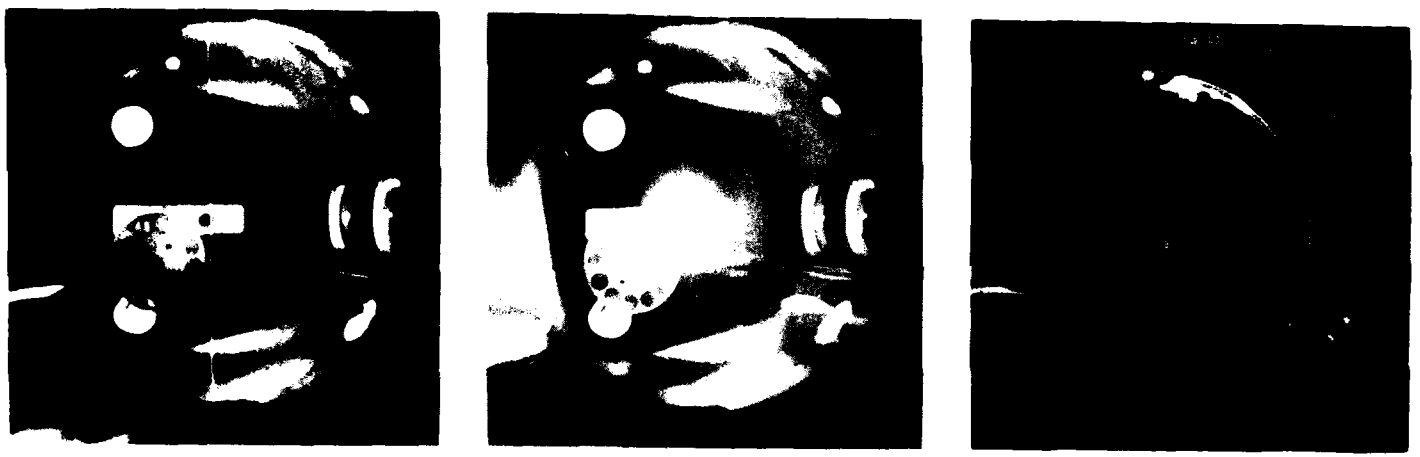

PELLET ONLY

PELLET IRRADIATED BY Nd:GLASS LASER

LASER ONLY

Fig. 12 — a. Still camera photograph of a deuterium pellet falling down the vertical HeNe laser beam; b. Same as "a" except that the pellet is vaporized by the Nd/G1 when it reaches the center of the chamber. c. A photograph taken to include the laser light with no pellet, to verify that the light burst in "b" is indeed due to a pellet.

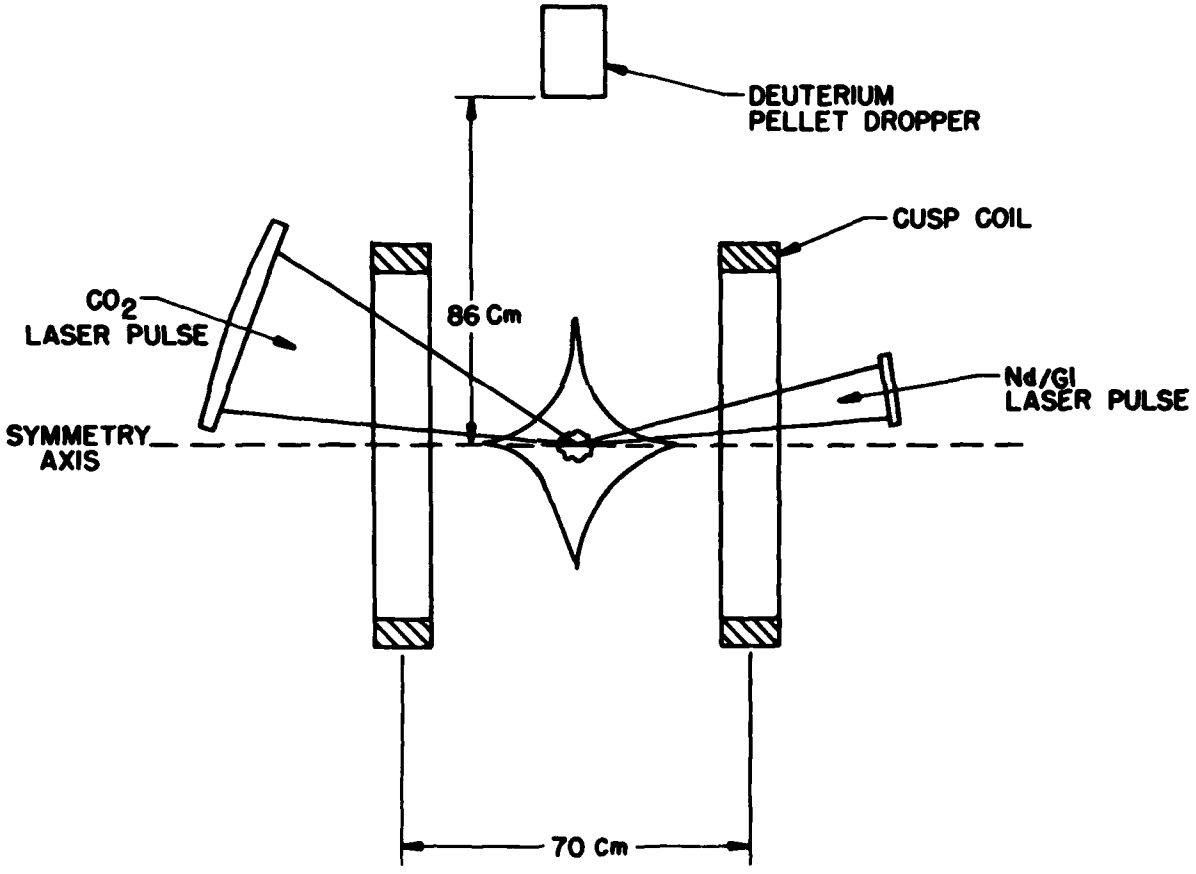

Fig. 13 — Schematic diagram of the Cusp experiment, showing plasma generation lasers, magnetic coils, and a pellet dropper.

DEUTERIUM PELLET EVAPORATION BY 100J Nd-GLASS LASER

Fig. 14 — Schlieren photographs of the expanding D_2 cloud after the pellet has been vaporized by the Nd/G1 laser.

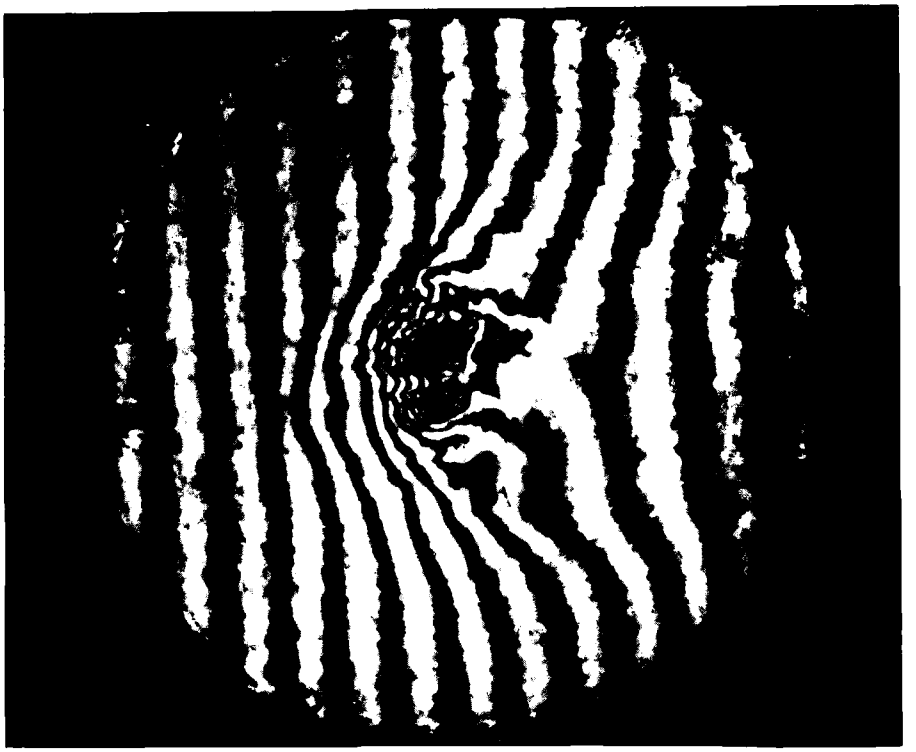

Fig. 15 — Holographic interferogram of the expanding plasma, taken 0.4 μ sec after the peak of the CO_2 laser.

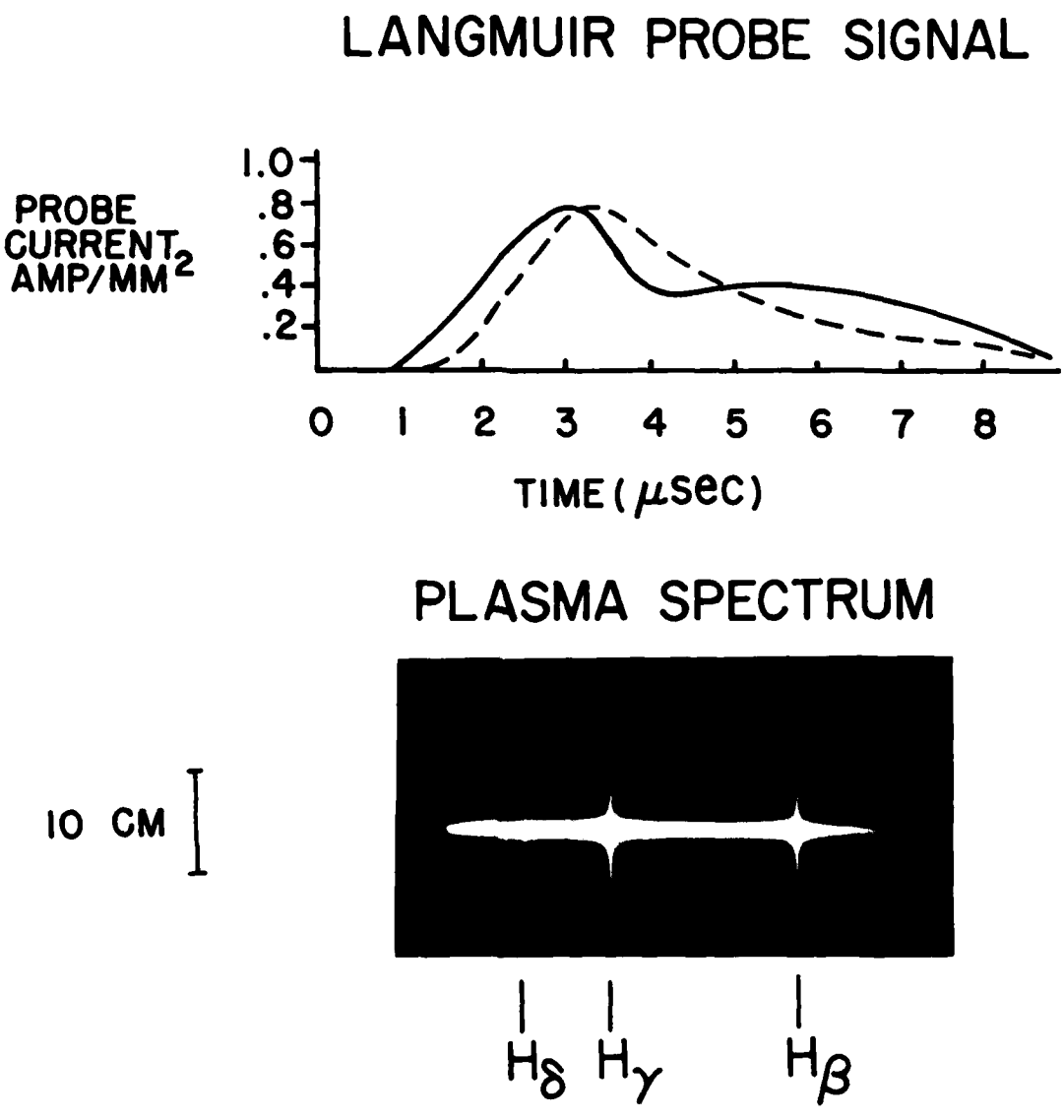

Fig. 16 — a. Ion saturation current (solid line) measured by a Langmiur probe located 30 cm from the center of the cusp, compared with an expanding Maxwellian plasma of 2 x 10^{19} ions and .7 x 10^{7} cm/sec average ion speed. Time is measured after the peak of the CO_2 laser. b. Spectrum of the plasma's light emission. Only H-lines are present.

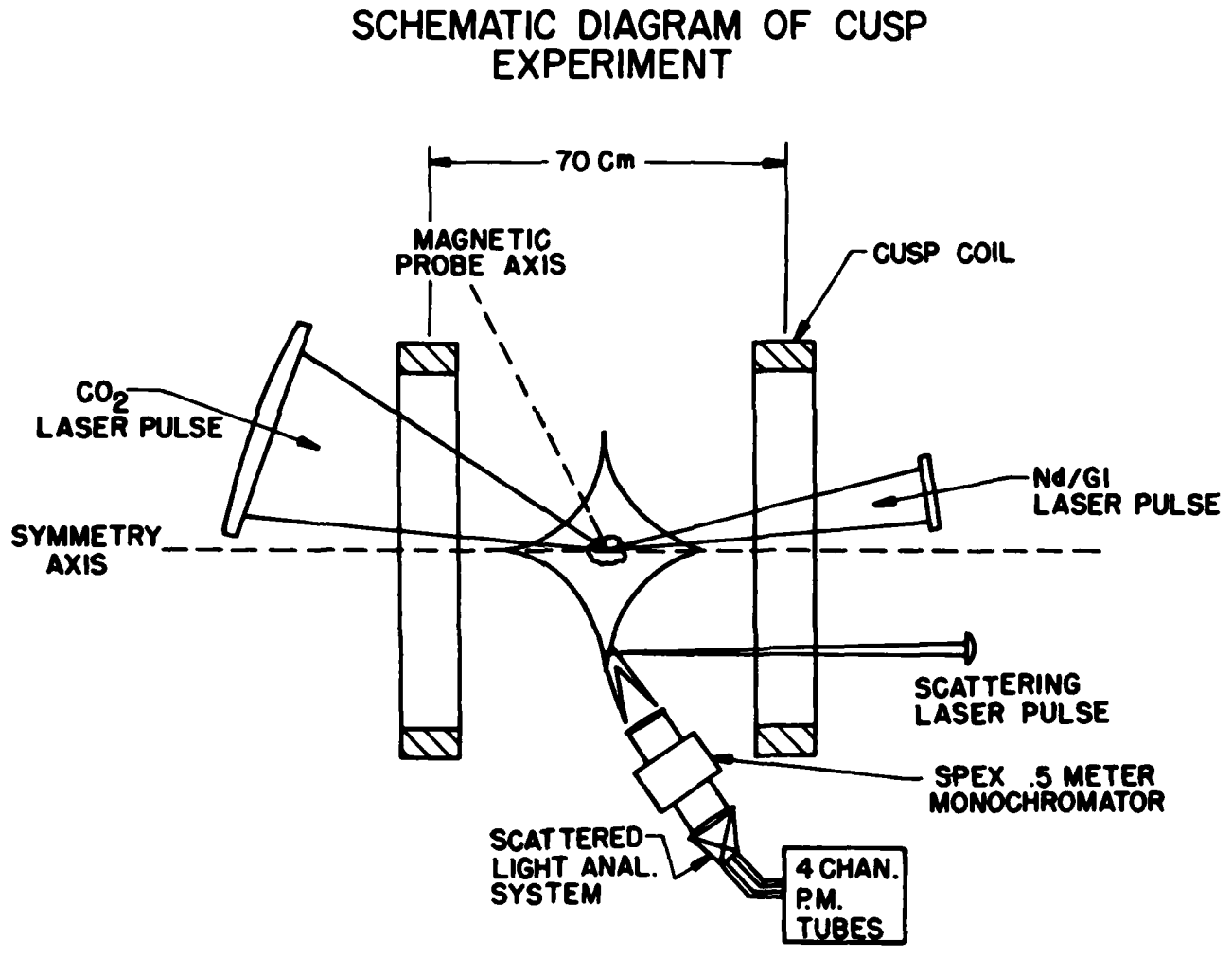

Fig. 17 — Schematic diagram of the Cusp experiment.

Fig. 18 — a. Still camera photograph of the interior of the vacuum chamber showing wall light emission at the ring cusp; b. Photograph of ring cusp light emitted at a glass window, taken from outside of the chamber, c. Streak photograph of light emitted at the same window. The duration of the light emission is of the order of 10 μsec.

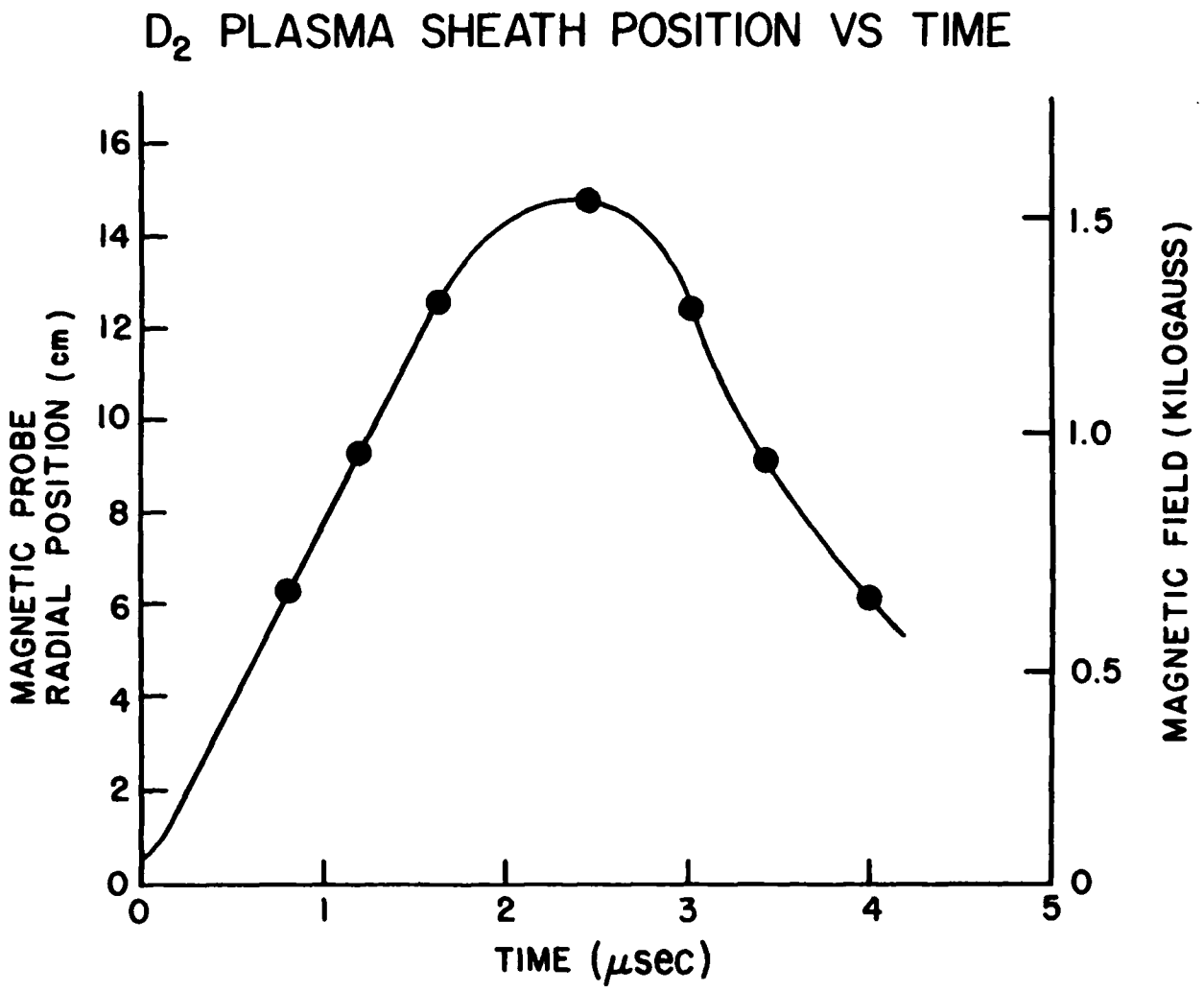

Fig. 19 — Graph of the radial position of the plasma-magnetic field interface versus time after the peak of CO_2 laser pulse. The position is measured along a radial line oriented 17° from the ring cusp.

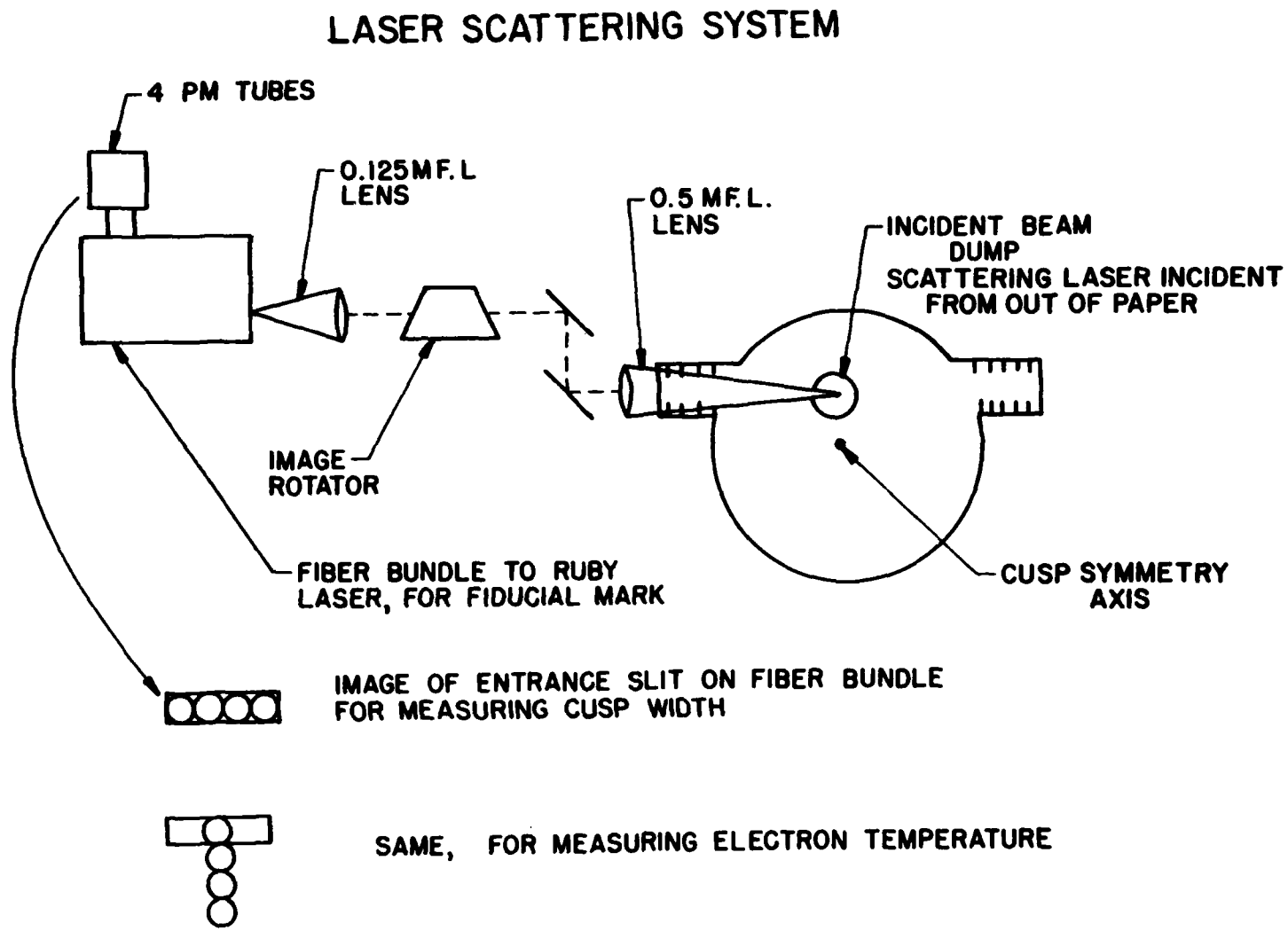

Fig. 20 — Schematic diagram of the laser scattering diagnostic system.

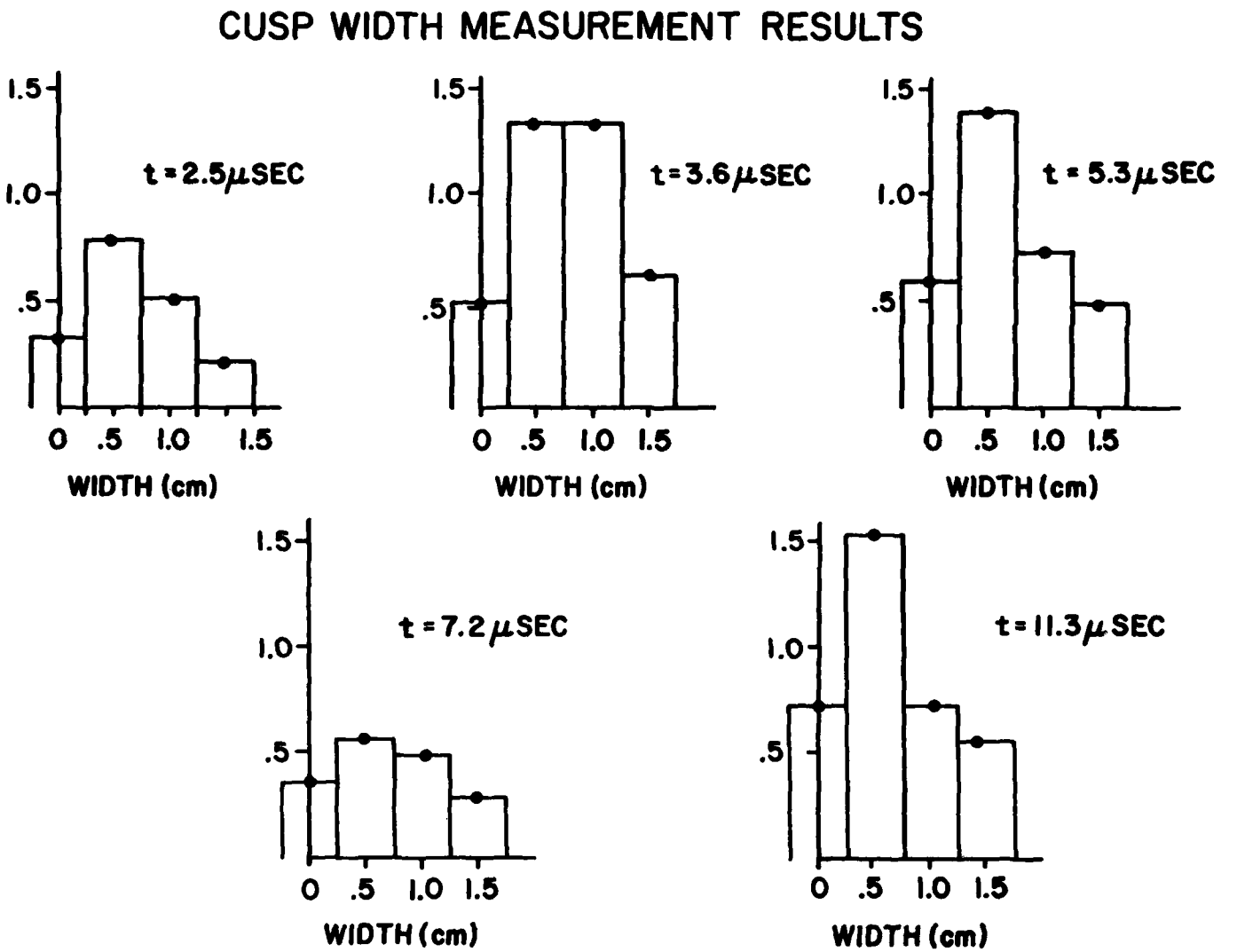

Fig. 21 — Results of the laser scattering cusp width measurements. Vertical axis is in units of $10^{15}cm^{-3}$.

SCATTERING SYSTEM OSCILLOSCOPE TRACES

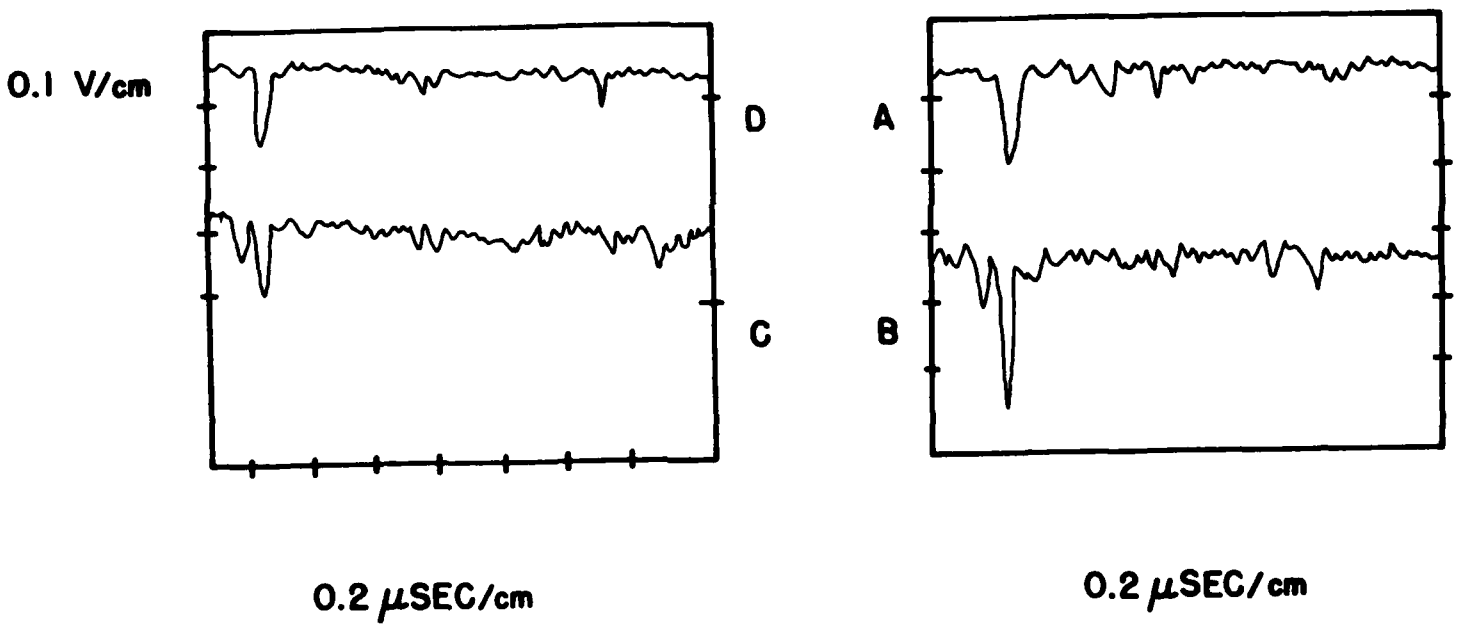

Fig. 22 — Scattering system oscilloscope traces. The large signal at τ = 0.25 μsec in each trace is the fiducial mark indicating the time the laser fires. The peak of the scattering signal occurs .07 μsec before the fiducial mark.

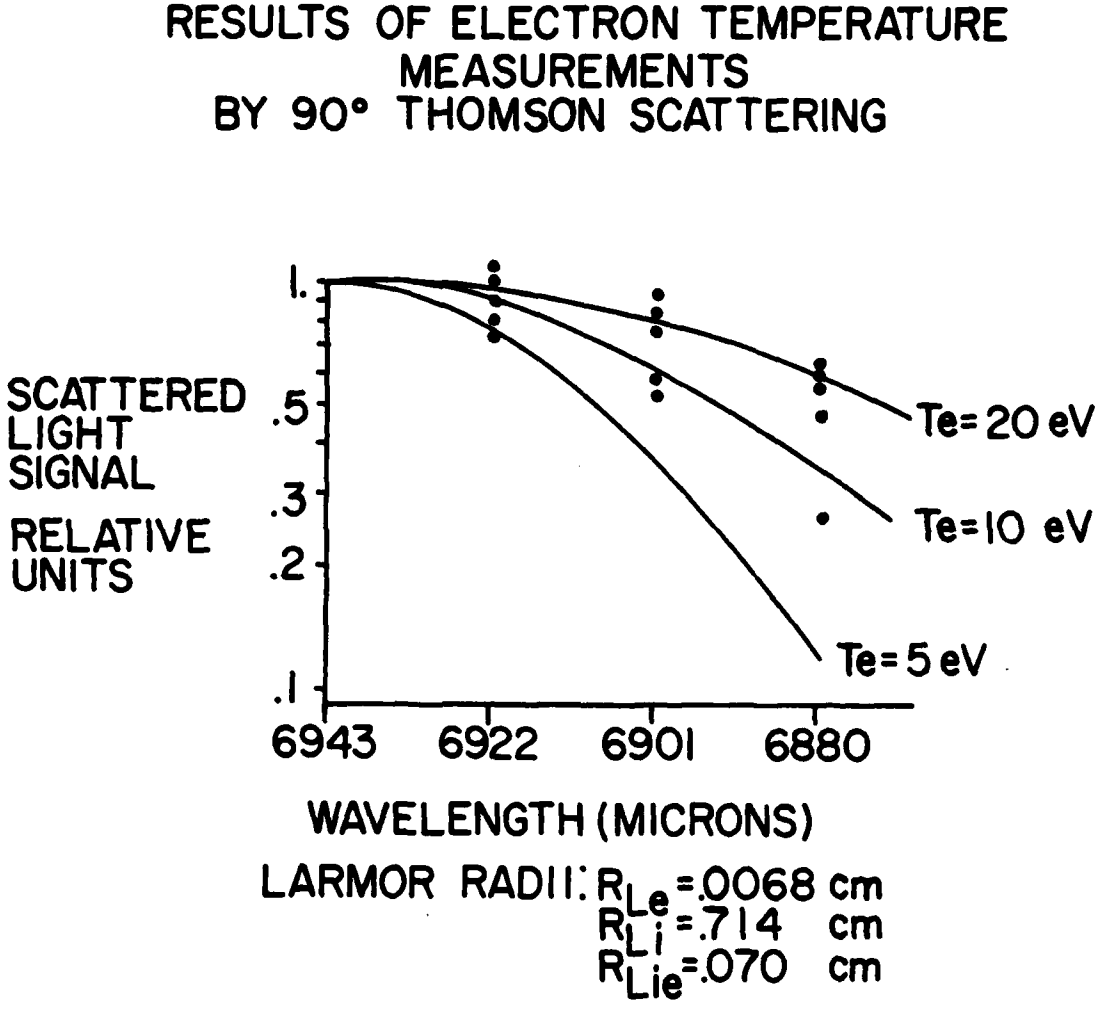

Fig. 23 — Results of electron temperature measurements of the cusp plasma by 90° laser scattering.

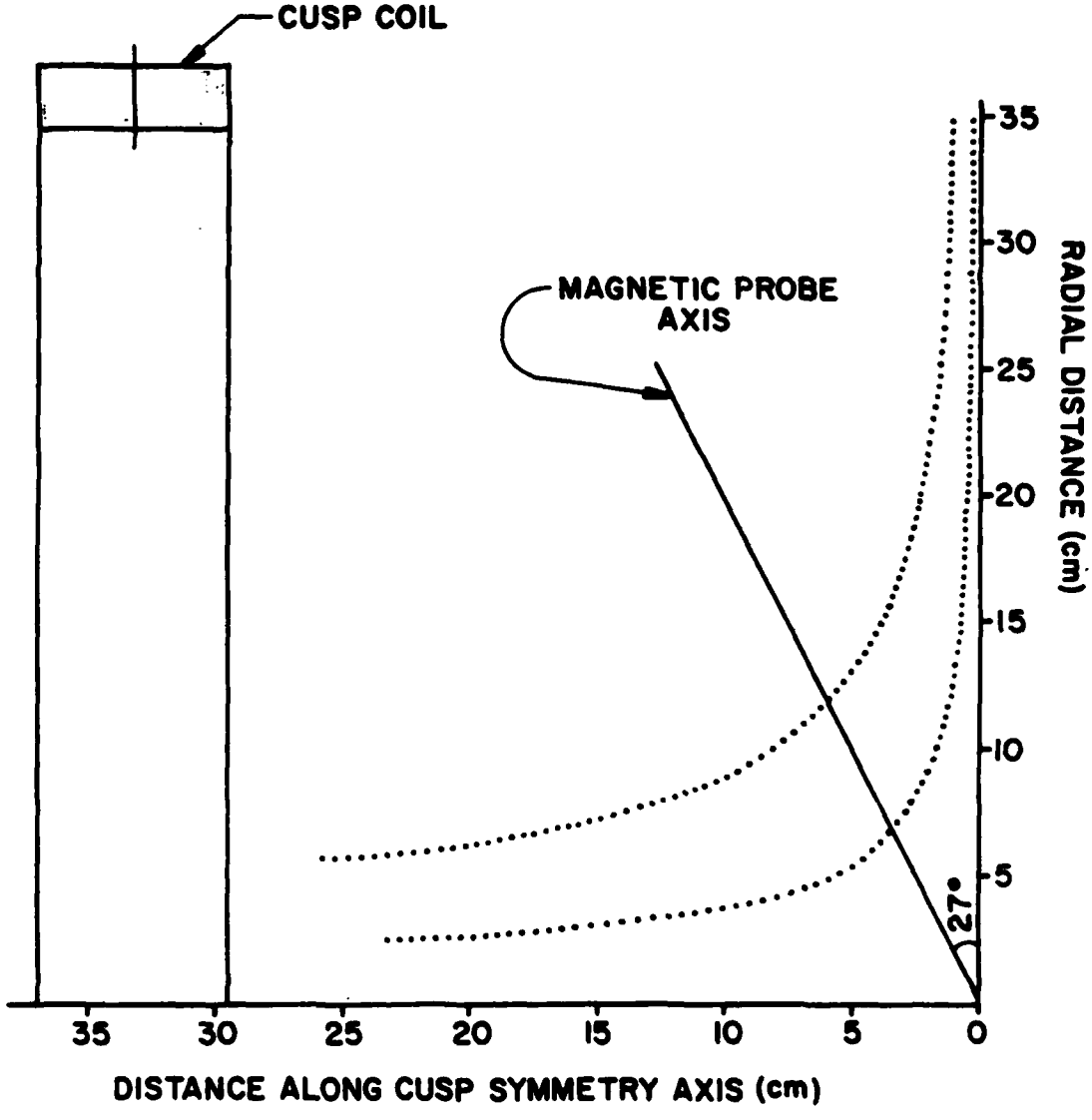

Fig. 24 — Magnetic field line plots of two cusp field lines, showing the relative positions of the movable magnetic probe and the cusp coils.

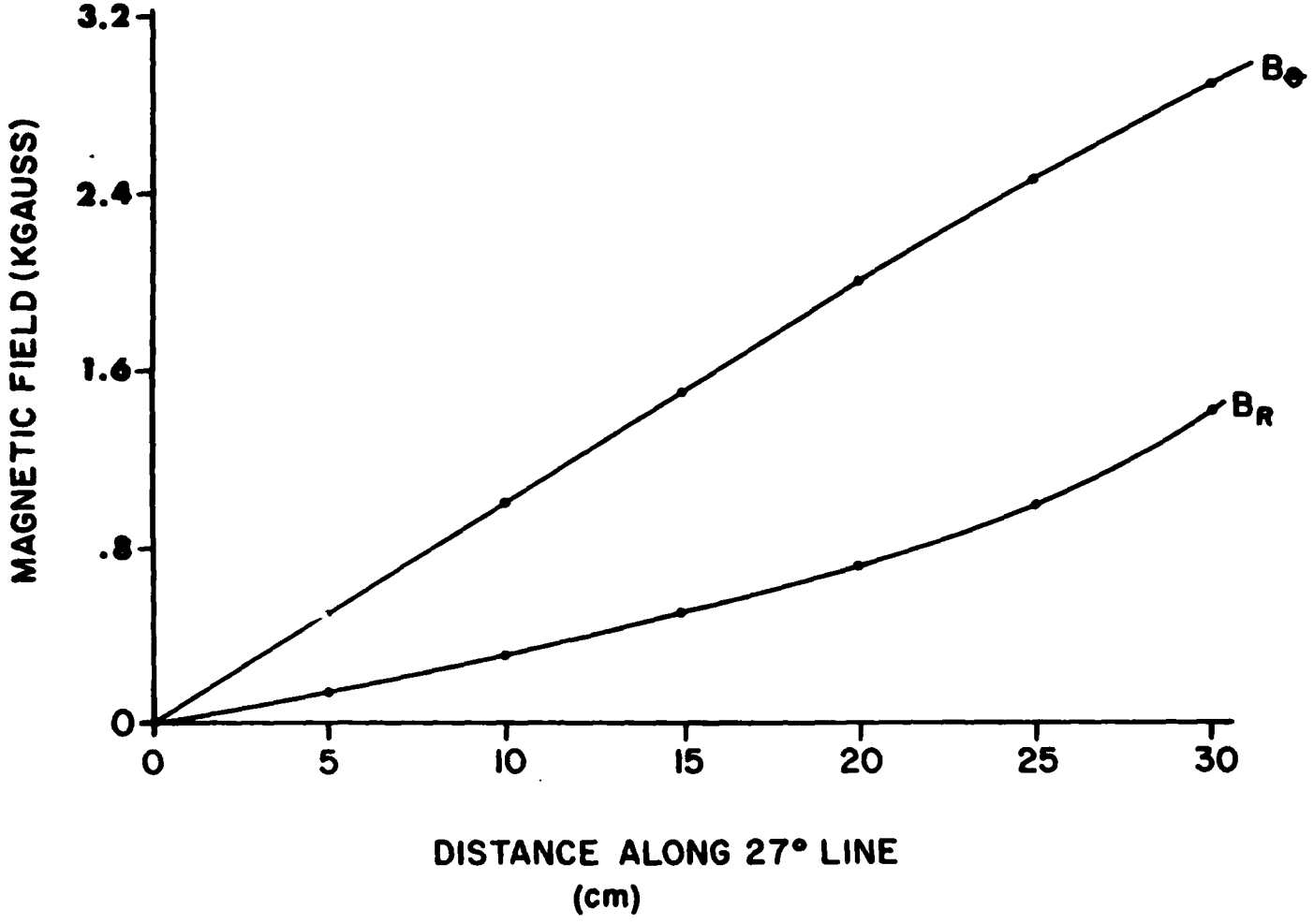

Fig. 25 — Plot of the magnetic field along the 27° axis of the magnetic probe. The upper curve is the component of the field perpendicular to the probe axis. The lower curve is the parallel component.

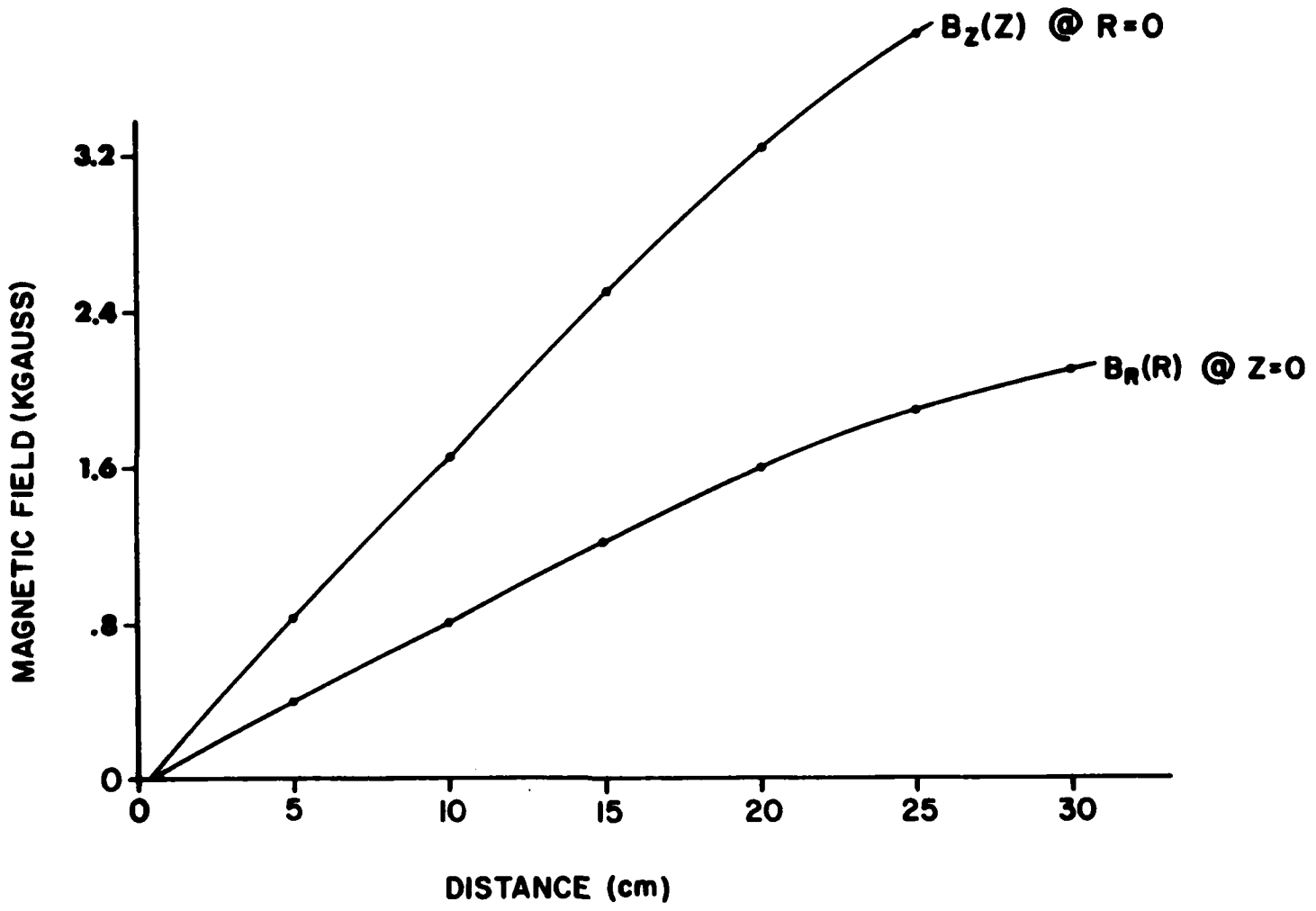

Fig. 26 — Plot the axial magnetic field along the cusp symmetry axis through the point cusp and a plot of the radial field through the ring cusp.